

國立交通大學

奈米科技研究所

碩士論文

奈米金表面修飾增加鍵結效率並應用於光電生物感

測器之研究

Nanoscale-Based Transduction for High-Efficiency of Biomolecular

Interactions and Optoelectronic Biosensor Application

研究生：游群芳

Chun-Fang Yu

指導教授：柯富祥 教授 Prof. Fu-Hsiang Ko

中華民國九十六年七月

奈米金表面修飾增加鍵結效率並應用於光電生物感
測器之研究

Nanosacle-Based Transduction for High-Efficiency of Biomolecular
Interactions and Optoelectronic Biosensor Application

研 究 生：游群芳

Student : Chun-Fang Yu

指 導 教 授：柯富祥 教授

Advisor : Prof. Fu-Hsiang Ko



國立交通大學

奈米科技研究所

碩 士 論 文

A Thesis

Submitted to Institute of Nanotechnology
College of Engineering
National Chiao Tung University
in partial Fulfillment of the Requirements
for the Degree of
Master
in
Nanotechnology
July 2007
Hsinchu, Taiwan, Republic of China

中華民國九十六年七月

摘要

近年來，跨領域的奈米科技發展的非常蓬勃，其中重要的應用之一便是結合半導體產業以及生物科技所產生的生物感測器。生物感測器首先必須將生物分子固定至半導體元件表面，然後靈敏且專一的偵測目標分子。本論文主要在於研究在選擇性的將生物分子組裝固定到矽相關材料的結構上面，並且利用化學或物理的方式使已經微小化的生物感測器中能產生更多的可反應表面積。

我們首先將表面以APTES修飾，固定螢光分子到氧化矽基材上，挑選出最合適於固定化的各個參數。之後我們成功的將金奈米粒子以及cysteamine相繼固定在二氧化矽上，進而誘導更多的生物分子鍵結，達到擴大輸出訊號的效益。此外，我們將固定化技術應用到一個嶄新金屬-半導體-金屬材料晶片上。利用系統中化學發光的反應，使光子轉變成電子訊號，進而證明晶片上已順利測定到目標生物分子。



Abstract

Significant development in nano-technology has been extensively devoted in recent years. One of the most important application is the development of biology sensor that can combine both the semiconductor industry and biological technology. Biosensors anchor the biology molecular onto the surface of semiconductor and detect target molecular distinctively. This thesis discloses the approach to grafting biology molecular onto the Si based surface and created more active area in these micro biosensors by physical and chemical methodologies.

We modified the surface with APTES, immobilized the fluorescent molecular onto the silicon based substrate, and obtained the best parameter which was the most suitable condition for anchoring process. After that, we sequentially anchored gold nano-particle and cysteamine on the silicon oxide to create much more binding sites for biological molecular. Therefore, we achieved the advantages of signal output enhancement.

Besides, we applied such grafting technique to a new metal-semiconductor-metal biochip. The grafting target biological molecule on the desired chip is successfully, and the evidence of the utilization of the chemical luminance reaction to transfer the photon into electric signal is also achieved.

Acknowledgment

首先，我要誠摯的感謝指導教授 柯富祥老師，老師悉心的教導使我得以一窺生物感測領域的深奧，不時的討論並指點我正確的方向，使我在這些年中獲益匪淺。老師對學問的嚴謹更是我輩學習的典範。

兩年裡的日子，實驗室裡共同的生活點滴，學術上的討論、言不及義的閒扯、讓人又愛又怕的宵夜、趕作業的革命情感、以及總是很有默契的一起去運動.....，感謝眾位學長、同學、學弟妹的共同砥礪(墮落?)，你/妳們的陪伴讓兩年的研究生活變得絢麗多彩。感謝俊淇、其昌、佳典、思豪、坤霖學長們不厭其煩的指出我研究中的缺失，且總能在我迷惘時為我解惑，也感謝志杰、奕儂、敬雅、誠樸、祐齊、立宇同學的幫忙，恭喜我們順利走過這兩年。實驗室的中書、宜生學弟、依秦、美榕、德玲學妹們當然也不能忘記，你/妳們的幫忙及搞笑我銘感在心。

感謝我最重要的好友們: 曉秋，智偉以及馥華，你們願意在我最需要的時刻出現，在我需要幫助的時候伸出援手，願意傾聽我的心事，我的畢業證書應該切一角分給你們才對。

安懿在背後的默默支持更是我前進的動力，沒有你的體諒、包容，相信這兩年的生活將是很不一樣的光景。也要感謝安懿的父母，你們的關心總是讓我感動萬分。

最後，謹以此文獻給我摯愛的雙親，以及我愛的人。

Contents

Abstract in Chinese.....	i
Abstract in English.....	ii
Acknowledgment.....	iii
Contents.....	iv
List of Figures.....	vi
List of Tables.....	ix
List of Scheme.....	x

Chapter 1: Introduction

1.1 General Introduction.....	1
1.2 Categories of Biosensor	
1.2.1 Electrochemical Transducers.....	1
1.2.2 Thermal Transducers.....	2
1.2.3 Piezoelectric Transducers.....	3
1.2.4 Optical Transducers.....	4
1.2.5 Field-Effect Transistor.....	7
1.3 Motivation.....	16
1.4 Thesis Organization.....	17



Chapter 2: Literatures Review

2.1 Chemiluminescence Biosensor.....	18
2.1.1 Principles of Enzyme Activated Chemiluminescence.....	21
2.2 Immobilization Technique.....	23
2.2.1 Cleland's reagent: DTT.....	25
2.3 Fundamentals of the MSM-PD.....	29

2.2.1 Current Transport Mechanism.....	32
Chapter 3: Experiments	
3.1 General Introduction.....	34
3.2 Experimental	
3.2.1 Self-assembling of B-epoxide on APTES for enhancing immobilization of streptavidin.....	39
3.2.2 Self-assembling of cysteamine on GNPs for enhancing immobilization of streptavidin.....	40
3.2.3 Chemilumescence type photo-sensor detection of HRP-catalyst luminol reaction...	42
Chapter 4: Results and Discussion	
4.1 Optimization of Self-assembly Parameters on Silicon Oxide Surface.....	47
4.2 Surface Modification by B Epoxide.....	53
4.3 Biotin-Streptavidin Conjugate with GNPs Assisted Modification.....	54
4.3.1 Studies with Fluorescence Microscopy and IPP software.....	57
4.3.2 Studies by UV-Visible.....	62
4.3.3 Investigating by Photo Diode.....	65
4.4 Surface Energy for of Biomolecule Immobilization.....	67
4.5 Biosensing of Streptavidin by Real Time Optical Biosensor.....	70
4.5.1 Real Time Sensing of Streptavidin by Detecting Chemilumescence Applysis.....	70
Chapter 5: Conclusions.....	75

List of Figures

Chapter 1: Introduction

Figure 1.1	3
Schematic of a typical thermoresistor device, as used as a biosensor in enzymatic reactions.	
Figure 1.2	4
Schematic diagram of a typical QCM.	
Figure 1.3	6
Schematic diagram of a biosensor based on surface plasmon resonance principle, (1) metal (Gold); (2) sensitizing layer; (3) sample solution (antigen) and (4) glass substrate. The device measures changes in the refractive index upon antigen-antibody binding.	
Figure 1.4	7
Reaction mode of luminol.	
Figure 1.5	8
Mechanism of alkaline-phosphatase-activated luminescence through the hydrolysis of the phosphate ester of adamant dioxetane.	
Figure 1.6	9
Classification of a material according to energy bands and interatomic spacing and the semiconductor band gap energy model.	
Figure 1.7	10
Energy bands through an MIS system as a function of the applied voltage V_G .	
Figure 1.8	11
Schematic of the insulated-gate field-effect transistor (IGFET): 1, p-type silicon substrate; 2, insulator; 3, gate metal; 4, n-type source; 5, n-type drain; 6, metal contacts to source and drain.	
Figure 1.9	12
Schematic of the gate in an IGFET: M, metal; I, insulator; S, semiconductor.	
Figure 1.10	13
Schematic of a field-effect transistor with a chemically sensing gate surface (CHEMFET)	

Chapter 2: Literatures Review

Figure 2.1	19
A simple Jablonski diagram showing some important radiative and non-radiative process and illustration of chemiluminescence.	
Figure 2.2	21
(a) The typical reaction of luminol, (b) the detailed reaction steps of luminol catalyzed by HRP.	
Figure 2.3	29
Schematic symbol of 1-D schematic, top view, and cross-section view.	

Figure 2.4.....	31
Schematic diagram of MSM-PD, charge distribution under low bias voltage, electric field distribution under low bias voltage and energy band diagram of MSM-PD.	
Figure 2.5.....	32
Current transport mechanism under forward bias.	

Chapter 4: Results and Discussion

Figure 4.1.....	48
Images of contact angle: (a) after treating with piranha solution and (b) after APTES process.	
Figure 4.2.....	50
The patterned wafer of silicon oxide/poly silicon was immobilized with rhodamine B isothiocyanate. The materials of dark and bright areas were poly silicon and silicon oxide, respectively. (a) APTES modified wafer reacts with rhodamine B isothiocyanate. (b) Fluorescence image of APTES/ rhodamine B isothiocyanate modified wafer.	
Figure 4.3.....	52
The images of fluorescence microscopy. (a) APTES/NHS-biotin (reaction time: 1 hour)/STA-Fitc (exposure time: 5 seconds); (b) APTES/NHS-biotin (reaction time: 6 hour)/STA-Fitc (exposure time :5 seconds)	
Figure 4.4.....	52
The images of fluorescence microscopy. (a) APTES/NHS-biotin (reaction time: 6 hour)/STA-Fitc (exposure time: 1 seconds) without blocking; (b) APTES/NHS-biotin (reaction time: 6 hour)/STA-Fitc (exposure time: 1 seconds) with blocking.	
Figure 4.5.....	54
The images of fluorescence microscopy of (a) without modification and (b) with modification by B epoxide.	
Figure 4.6.....	56
The SEM image of gold nanoparticle and number-diameter bar chart of gold nanoparticle.	
Figure 4.7.....	57
Absorbance spectra of differ size of gold nanoparticles.	
Figure 4.8.....	58
The diagram of brightness quantification procedure.	
Figure 4.9.....	60
The bar chart of brightness after quantification.	
Figure 4.10.....	61
The bar chart of brightness after quantification (with DTT assisted modification).	
Figure 4.11.....	62
The bar chart of brightness after quantification. The graft of streptavidin-Fict; without GNPs, with GNPs but without DTT and with GNPs plus DTT.	
Figure 4.12.....	63

The OD value versus wavelength of absorption. Chemiluminescence detection system.	
Figure 4.13	64
The OD value of luminal decay with reaction time. Conjugation of streptavidin-HRP without (a) and with (b) GNPs and cysteamine assistant.	
Figure 4.14	64
The OD value of luminal decay with reaction time. Conjugation of streptavidin-HRP without (a) and with (b) GNPs and cysteamine assistant.	
Figure 4.14	66
Real time measurement of chemiluminescence substrate. Without GNPs assistant immobilization; (b) with GNPs assistant immobilization.	
Figure 4.15	71
Chemiluminescence detection system.	
Figure 4.16	72
Current of MSM-PD after piranha solution.	
Figure 4.17	72
Current of MSM-PD after self assembling of APTES.	
Figure 4.18	73
Current of MSM-PD after binding with NHS-bioth.	
Figure 4.19	73
Current of MSM-PD after conjugating with streptavidin.	
Figure 4.20	74
Real time measurement of adding chemiluminescence substrate of HRP (for detecting the streptavidin).	

List of Tables

Chapter 1: Introduction

Table 1.1.....14

Types of transducers, their characteristics and application.

Chapter 2: Literatures Review

Table 2.1.....23

The comparison between fluorescence and chemiluminescence methods.

Chapter 4: Results and Discussion

Table 4.1.....68

The advancing contact angles for water, ethylene glycol (EG), and diiodomethane (DIM) on various modified surfaces.

Table 4.2.....69

The corresponding surface free energies.



List of Schemes

Chapter 1: Introduction

Scheme 1.1	14
Biocomponent and transducers employed in construction of biosensors.	

Chapter 2: Literatures Review

Scheme 2.1	26
Thiol-containing disulfide reductants reduce disulfide groups through a multistep process producing a mixed intermediate	
Scheme 2.2	27
DTT is highly efficient at reducing disulfides, since a single molecule can reduce the intermediate mixed disulfide by forming a ring structure	
Scheme 2.3	27
Regio- and stereocontrolled opening of cyclitol epoxides. Synthesis of cyclitol Analogues by regioselective C1 opening of the starting epoxide.	
Scheme 2.4	28
Lithium promoted opening of cyclitol epoxides 1 (R=H) and 2 (R=Bn).	
Scheme 2.5	28
Synthesis of cyclitol analogues by regioselective C1 opening of the starting epoxide.	

Chapter 3: Experiment

Scheme 3.1	40
The steps of immobilization of biotin with streptavidin and follow up observation.	
Scheme 3.2	42
The steps of immobilization of biotin with streptavidin and follow up observation.	
Scheme 3.3	44
Process flow chart of MSM-PD fabrication.	
Scheme 3.4	46
Diagram of MSM photo sensor or photodiode with chemiluminescence reaction.	

Chapter 4: Results and Discussion

Scheme 4.1	48
The process flow of optimization of self assembling.	
Scheme 4.2	51
Schematically illustration of NHS-biotin reacts with amino group.	
Scheme 4.3	53
The process flow of modification by B epoxide.	

Scheme 4.4.....55
he process flow of modification by gold nanoparticles and cysteamine.



Chapter 1: Introduction

1.1 General Introduction

The interdisciplinary study of biology, chemistry, and electronics is more and more important than ever before. Combining biotechnology and semiconductor technology, various types of biochips and biosensors have now been developed to detect and monitor-specific binding of biomolecules on the solid-state substrates [1]. The choice of suitable way for the purpose of biomolecular immobilization has become an increasingly important biological tool in recent years. Genomics and proteomics research has elucidated many new biomarkers that have the potential to greatly improve disease diagnosis [2].

Biosensors are a sub group of chemical sensors in which are comprises a biorecognition molecule immobilized over a signal transducer to give a reagentless analytical device. The bio-recognition molecule, such as an enzyme, antibody, sequence of DNA, peptide or even a micro-organism, provides the biosensor with its selectivity for the target analyte so that the molecule of interest can be picked out by the biosensor from a matrix of many other molecules. The signal transducer determines the extent of the bio-recognition event and converts it into an electronic signal, which can be outputted to the end user. Common transducers include amperometric electrodes, optical waveguides or mass sensitive piezoelectric crystals [3].

These devices represent a promising tool for bio-analysis due to the possibility to fulfill some demands that the classic methods of analysis do not attain. Original characteristic turns the biosensors technology to be a possible methodology for real sample application. Some advantages such as high selectivity and specificity, relative low cost of construction and storage, potential for miniaturization, facility of automation and simple and portable equipment construction are proposed for a fast analysis and biomolecular monitoring. [4]

1.2 Categories of Biosensor

According to the detector devices, there are several types of transducers. Scheme 1.1 summarizes these biocomponents and transducers.

1.2.1 Electrochemical Transducers

An electrochemical biosensor, according to the IUPAC definition, is a self-contained

integrated device, which is able to provide specific quantitative or semi quantitative analytical information using a biological recognition element (biochemical receptor) which is retained in direct and spatial contact with the transduction element [5]. Biosensors based on electrochemical transducer have the advantage of being economic and present fast response; the possibility of automation allows application in a wide number of samples. The electrochemical biosensors can be classified in conductimetric, impedimetric, potentiometric and amperometry.[6]

There are three basic electrochemical processes that are useful in transducers for sensor applications:

- Potentiometry: the measurement of a cell potential at zero current.
- Voltammeter (amperometry): in which an oxidizing (or reducing) potential is applied between the cell electrodes and the cell current is measured.
- Conductometry: where the conductance (reciprocal of resistance) of the cell is measured by an alternating current of bridge method.

1.2.2 Thermal Transducers

Biosensors with thermal transducers are based on the monitoring of the energy changed, under the heat form, over time, which occurs in a chemical reaction catalyzed by enzymes or microorganisms (Figure 1.1). However, the heat cannot be perfectly confined in an adiabatic system and always presents a loss of information since the produced heat is partly wasted by irradiation, conduction or convection. These devices can operate with continuous flow and are insensitive to the optical and electrochemical properties of the sample. [7]

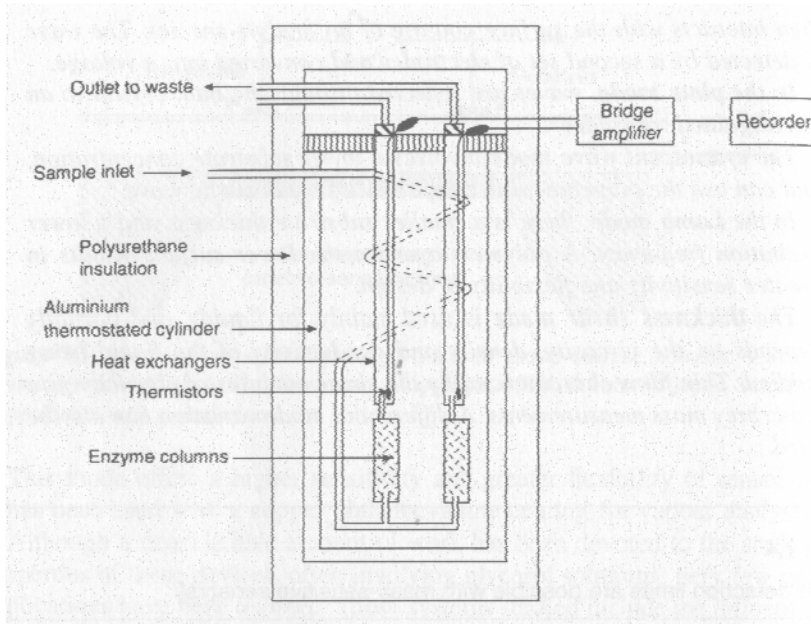


Figure 1.1. Schematic of a typical thermoresistor device is used as a biosensor in enzymatic reactions.[8]

1.2.3 Piezoelectric Transducers

Piezoelectric sensors are devices that transduce the measured physical parameter in the form of mechanical strain into variations of electric charge. Piezoelectric devices are used to measure physiological displacements and pressures and record heart sounds, as well as for the generation and reception of ultrasound (used to visualize body organs). When mechanically strained, piezoelectric materials generate an electric charge and a potential. Conversely, when an electric potential is applied to the piezoelectric material, it physically deforms. When an asymmetrical piezoelectric crystal lattice is distorted, a charge reorientation takes place, which causes a relative displacement of negative and positive charges. These displaced internal charges induce surface charges of opposite polarity on opposite crystal sides. Surface charge is determined by the potential difference between the surfaces. The theoretical foundation for the use of piezoelectricity was first proposed by Raleigh (1885) [9], but the first thorough investigation was by Jacques and Pierre Curie in 1880 [10]. A quartz crystal microbalance (QCM) consists of a thin quartz disk with electrodes plated on it as can be seen in Fig.1.2. However, this kind of transducer is too sensitive so lend huge noises. [4]

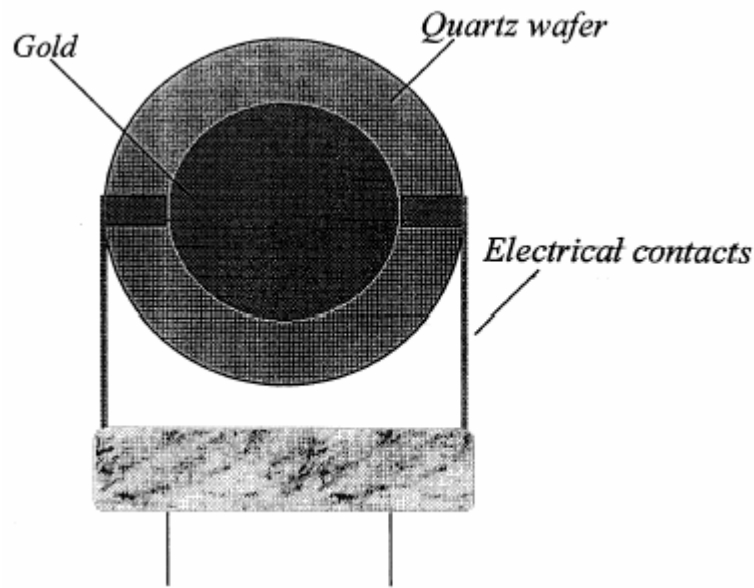


Figure 1.2. Schematic diagram of a typical QCM.[11]

1.2.4 Optical transducers

Biosensor operation with optical transducer is receiving considerable attention nowadays, and the main type of photometric behaviour which has been exploited in biosensor application is listed as follows:

- Ultraviolet–Visible absorption
- Fluorescence/phosphorescence emission
- Bio/chemiluminescence
- Internal reflection spectroscopy (IRS)
- Laser light scattering method

Optical sensors, initially, developed for oxygen, carbon dioxide and pH using acid-base indicators (Seitz, 1988) have been extended for the construction of fluorescent and luminescent optrodes[12]. Optrodes are constructed with an immobilized selective biocomponent at one end of an optical fiber, with both the excitation and detection components located at the other end. The change in the intensity of absorbed or emitted light from an indicator that can in turn interact with the selective biocomponent is the principle the pH, pO₂ and pCO₂ fiber-optic probes that achieve transduction via the indicator alone. This change is directly proportional to the amount of analyte present in the sample. The principle of these fiber-optic probes is the total internal

reflection (TIR) phenomenon in a light guide using evanescent waves, an electromagnetic wave that exists at the surface of many forms of optical waveguides, to measure changes in refractive index at the sensor surface. TIR-based biosensors make use of the evanescent wave penetrating only a fraction of a wavelength into the optically rare medium when light coming from an adjacent denser medium is incident on the interface at an angle above the critical angle. Changes in the surface refractive index or absorptivity reduce the transmission of light through the guide.

Another optical TIR-based biosensor that internal reflection in a light guide is SPR (surface plasmon resonance). SPR devices combine an evanescent wave detector with a biocomponent, generally, an antibody. The SPR method is a charge-density oscillation that may exist at the interface of two media with dielectric constants of opposite sign, for instance, a metal and a dielectric. An SPR optical sensor, generally, comprises an optical system, a transducing medium which interrelates the optical and (bio)chemical domains, and an electronic system supporting the optoelectronic components of the sensor and allowing data processing, energy carried by photons of light can be coupled or transferred to electrons in a metal. This coupling results in the creation of a plasmon, a group of excited electrons on the surface of the metal. The intensity of the plasmon is influenced by the type of metal and the environment of the metal surface. Changes in chemical properties within the range of the plasmon field (such as the protein interaction in antibody–antigen binding) cause changes in plasmon resonance. These changes can be measured as a change in the angle of incidence or shift in the wavelength of light absorbed and can be measured as a change in the SPR signal (expressed in resonance units, RU). Most SPR instruments measure changes in the angle of incidence. A SPR-based biosensor specimen is tested for its adsorption to a covalently immobilized molecule by surface sensitive optical techniques. The amount of adsorption is measured as a function of time and results are generated in the form of a sensogram that shows the response units measured as a consequence of the adsorption (Homola, Yee, & Gauglitz, 1999) [13].

SPR biosensors are easy to use, label free, and can assay crude samples without purification (Homola et al., 1999) [14], but the whole SPR system is very expensive. Figure 1.3 shown an SPR immunosensor that consists of a prism on a glass slide carrying a thin metal layer. The sensitizing antibody layer is in direct contact with the antigen or analyte to be determined. The changes in the refractive index can be monitored as a shift in the angle of the total absorption of incident light on a metal layer carrying the antibody.

Optical sensors make use of bioluminescent bacteria as *Vibrio fischeri* or *Vibrio harveyi* or chemiluminescent substances as luminol in combination with oxidoreductases for direct measurement. Optical luminescent biosensors have application in the control of fermentative processes, alcohol and in the determination of carbohydrates [15~18].

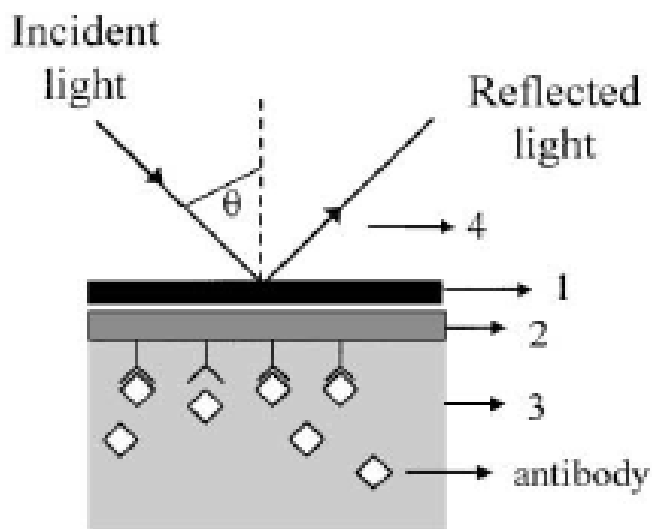


Figure 1.3. Schematic diagram of a biosensor based on surface plasmon resonance principle, (1) metal (Gold); (2) sensitizing layer; (3) sample solution (antigen) and (4) glass substrate. The devices measures changes in the refractive index upon antigen-antibody binding.[4]

Chemiluminescence occurs as a result of the oxidation of certain substances, usually with oxygen or hydrogen peroxide, producing visible light in the absence of any exciting illumination. The best known of these substances is luminol, shown in Figure 1.4. There are other more complex substance which will react in a similar way.

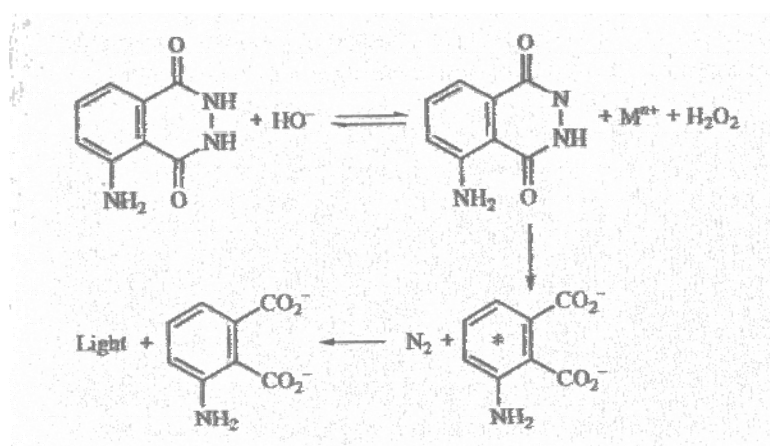


Figure 1.4. Reaction mode of luminal. [8]

The luminal is normally used as label. This can be employed in any assay involving oxygen, hydrogen peroxide or peroxidase. It is particularly useful with immunoassay. However, the sensitivity is limited because the quantum yield is only 1%. The most important advantage of chemiluminescence is that no external light source is needed, the sensor can connect directly to the photodiode

A recent example of a new type of chemiluminescence system involves adamantyl dioxetane phosphate (Figure 1.4) which can be hydrolysed under the influence of alkaline phosphatase to form the adamantyl dioxetane anion, which is unstable and fluoresces. The fluorescence lifetime is several minutes, unlike the more conventional type of luminescence, the structure of the materials involved and the mechanism of the fluorescence process are shown in Fig. 2.38. Such behavior could be used in many types of assay which involve phosphate ester hydrolysis using alkaline phosphatase. The adamantyl dioxetane phosphate could be allowed to compete with other organic phosphates for the phosphatase.

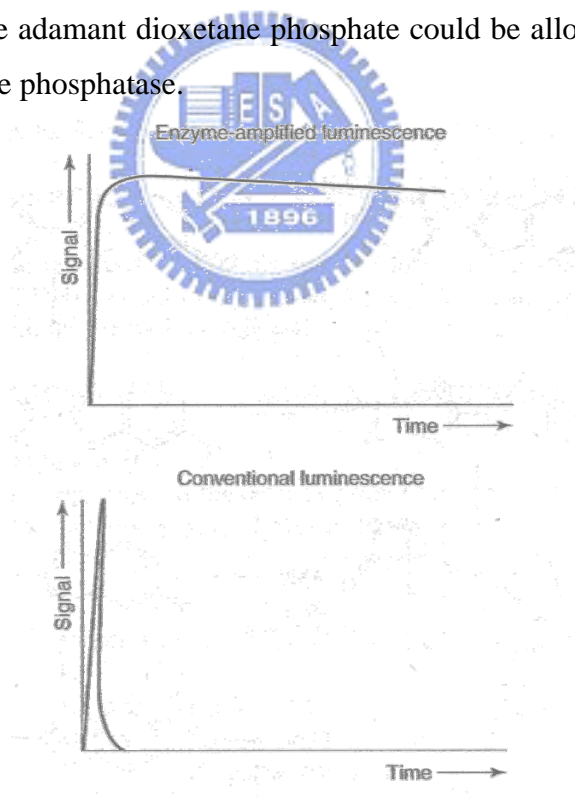


Fig.1.5. Mechanism of alkaline-phosphatase-activated luminescence through the hydrolysis of the phosphate ester of adamant dioxetane. [19]

1.2.5 Field Effect Transistor

Field-effect transistors (FETs) are devices in which a transistor amplifier is adapted to be a miniature transducer for the detection and measurement of potentiometric signals, produced by a potentiometric sensor process on the gate of the FET. A separate reference electrode is also needed. Circuit wiring is minimized, so that in addition to miniaturization, electronic noise is greatly reduced and sensitivity is increased. The FET device can be part of an integrated- circuit system leading to the read-out, or to the processing of the analytical data.

1.2.5.1 Semiconductors - Introduction

Materials can be classified as metals, non-metals or semiconductors. Generally metals are good conductors of electricity, while non-metals are bad conductors i.e. they behave as insulators. Semiconductors come somewhere in between. The differences can be seen in the way that they form energy levels. Non-metal atoms form discrete bonding and anti-bonding molecular orbitals when they combine to form molecules. The bonding orbitals contain the bonding electrons while the anti-bonding orbitals are empty, unless electrons are promoted into these by excitation. The energy space between these levels is 'forbidden' and is therefore unoccupied. In metals, there are overlapping energy bands and so there is no forbidden region. Electrons can move freely throughout the bands, thus leading to their high conductivities. Semiconductors form energy bands, although in this case they are separated by a forbidden region. The lower band is known as the valence band (VB), while the upper band is called the conduction band (CB). The energy gap between the two is called the band gap. These features are shown in Figure 1.6.

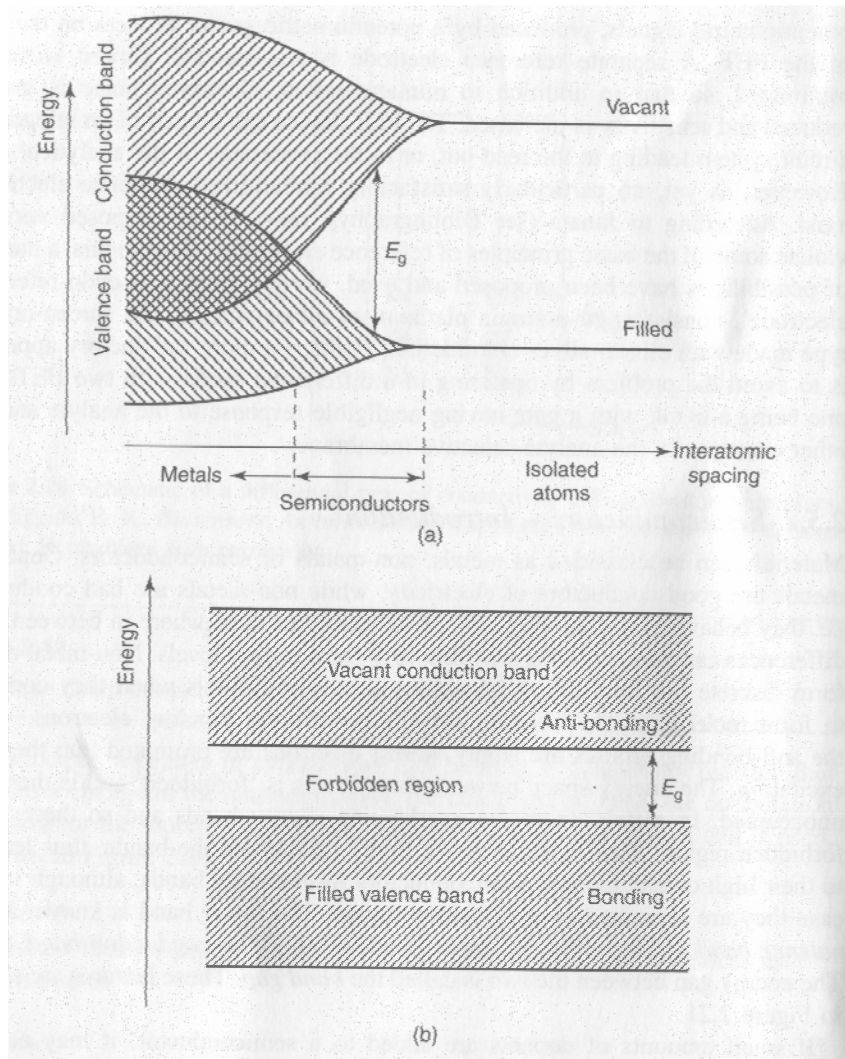


Fig.1.6. (a) Classification of a material according to energy bands and interatomic spacing (b) The semiconductor band gap energy model. [20]

If small amounts of dopants are added to a semiconductor, it may acquire an excess of electrons to give a p-type semiconductor, or a deficit of electrons (excess of holes) giving an n-type semiconductor. Fifth-row elements (in the anodic Table), such as arsenic, form p-type semiconductors, while third-row elements, like gallium, will form n-type semiconductors.

The Fermi level (E_F) is the point where the probability of filling the (energy) band is 0.5. For an undoped (intrinsic) semiconductor, this will be half-way between the VB and the CB, while for a doped semiconductor, E_F lies nearer to the VB in p-doped materials and nearer to the CB in n-doped materials.

A common arrangement of semiconductors for sensor applications is the metal-insulator-semiconductor (MIS) system. If no potential is applied the, The Fermi level is the

same across the metal to the semiconductor. However when a potential is applied the levels on the two sides separate. The system then behaves like a capacitor and charges build up on each side. Figure 1.7 shows the energy levels across a p-type

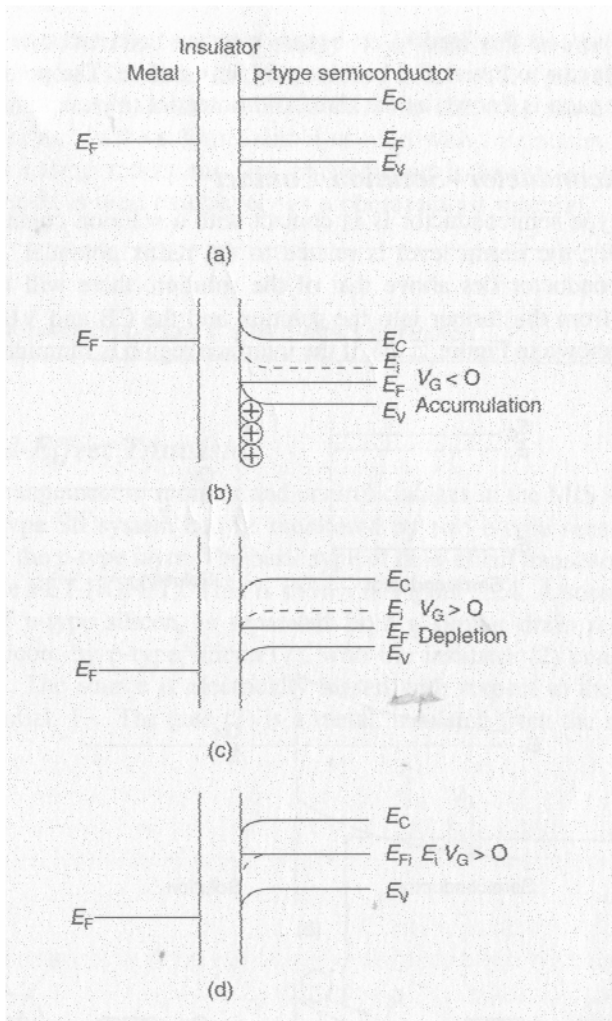


Figure 1.7. Energy bands through an MIS system as a function of the applied voltage V_G . [20]. semiconductor. It also shows the effect of applying a potential (a gate voltage, V_G) across the MIS system. With a small negative potential ($V_G < 0$), there is an accumulation of electrons at the metal/insulator (M/I) interface, and of holes (positive charges) at the semiconductor/insulator (S/I) interface. E_F is shifted towards the VB lower than the value in the metal by an amount equal to V_G and the energy levels near the semiconductor become bent upwards to compensate for this. With a small positive potential ($V_G > 0$), there is a depletion effect as positive holes are repelled from the S/I interface. In this case, the VB and CB bend downwards to compensate for this. If V_G is further increased, eventually the hole and electron concentrations near the interface become

equal. Now, the Fermi level is again midway between the VB and the CB - equivalent to the intrinsic level (Figure 1.7 (d)). Further increases in potential beyond the level lead to an excess electron concentration, thus causing the semiconductor to invert and become n-type in nature. The potential required to cause inversion is known as the threshold potential (V_T).

1.2.5.2 Field- Effect Transistor

This is an arrangement to monitor and control changes in the MIS system. Inversion at a p-type S/I system can be monitored by two n-type sensors placed on either side of the p-type layer. The basic type of field-effect transistor (FET) is the insulated-gate FET (IGFET). This is shown in Figure 1.8. A source region (4), consisting of n-type silicon, is separated from a similar drain region (5), also of n-type silicon, by p-type silicon (1), with the insulator (2) consisting of silicon dioxide. The source is electrically biased with respect to the drain by the applied potential, V_D . The gate (3) is a metal, insulated from the rest, so that it forms a capacitor sandwich, a metal/insulator/semiconductor (MIS) arrangement as shown in Figure 1.9.

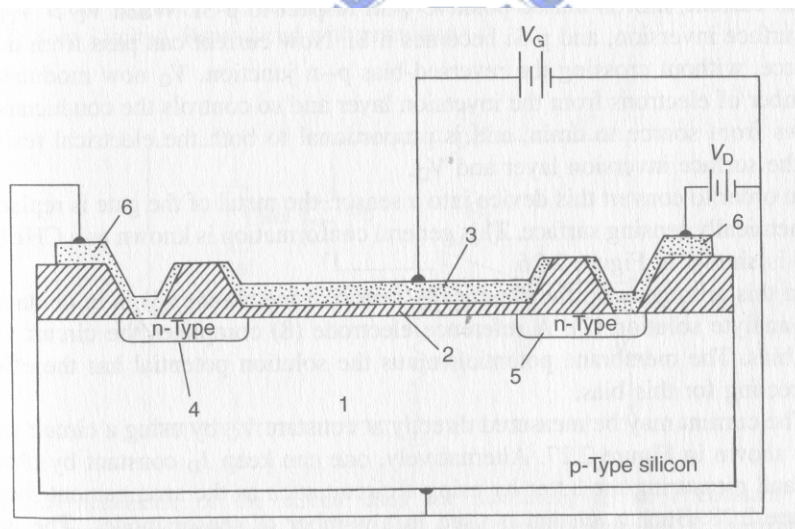


Figure 1.8. Schematic of the insulated-gate field-effect transistor (IGFET): 1, p-type silicon substrate; 2, insulator; 3, gate metal; 4, n-type source; 5, n-type drain; 6, metal contacts to source and drain. [19]

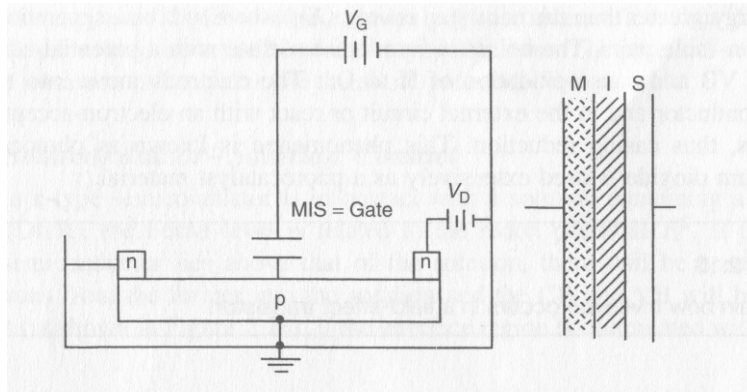


Figure 1.9. Schematic of the gate in an IGFET: M, metal; I, insulator; S, semiconductor. [19]

This gate region is charged with a bias potential V_G . The current from the drain (5) to the source (4), I_D , is measured. There is also a threshold potential, V_T , at which silicon changes from p-type to n-type, and inversion occurs. With a small positive V_D and $V_G < V_T$, silicon (1) remains in the p-state, and there is no drain current; n-Si is biased positive with respect to p-Si. When $V_G > V_T$, there is surface inversion, and p-Si becomes n-Si. Now current can pass from drain source, without crossing the reversed-bias p-n junction. V_G now modulates the number of electrons from the inversion layer and so controls the conductance. I_D flows from source to drain, and is proportional to both the electrical of the surface inversion layer and V_D .

In order to convert this device into a sensor, the metal of the gate is replaced a chemically sensing surface. This general conformation is known as a CHEMFET and is shown in Figure 1.10.

In this arrangement, the chemically sensitive membrane (3) is in contact the analyte solution (7). A reference electrode (8) completes the circuit via the V_G bias. The membrane potential minus the solution potential has the effect correcting for this bias.

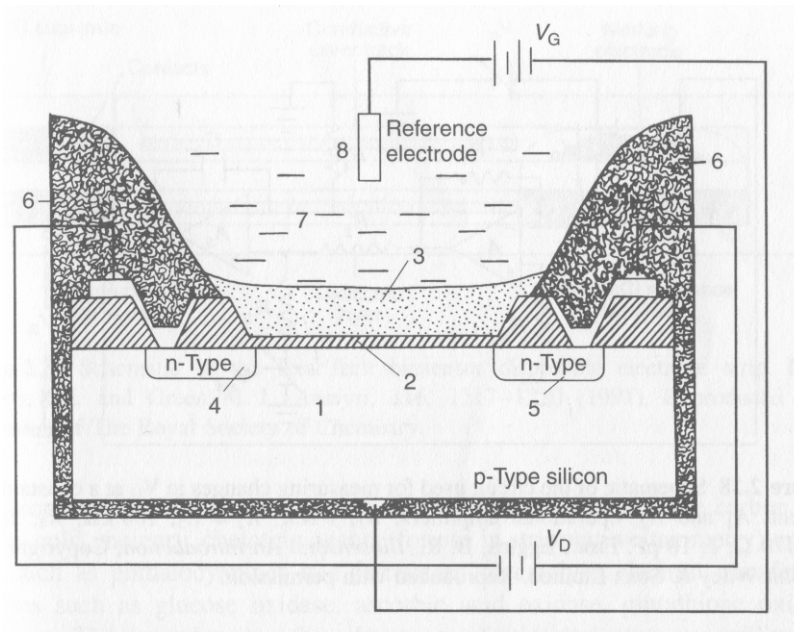
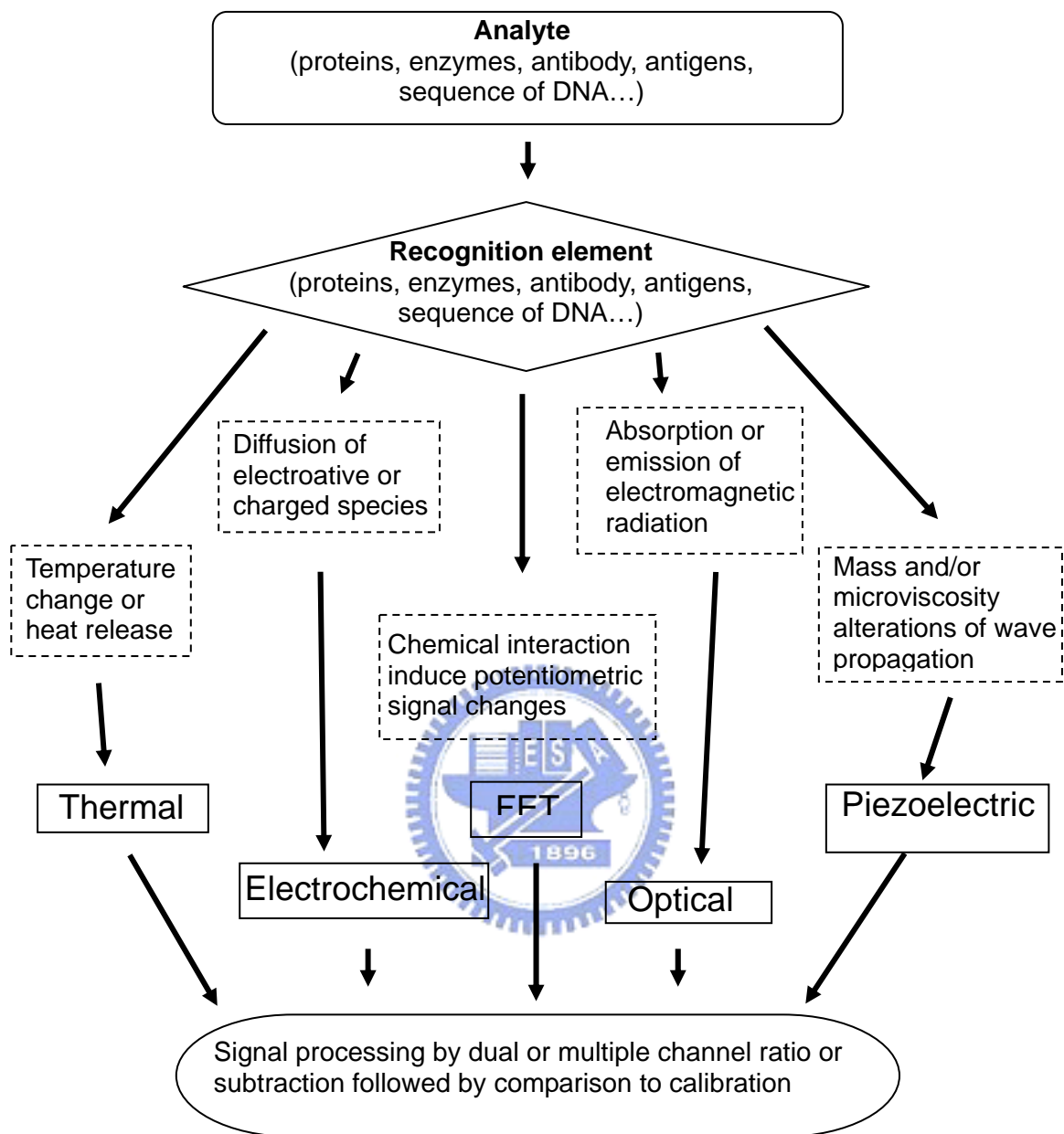


Figure 1.10 Schematic of a field-effect transistor with a chemically sensing gate surface (CHEMFET): 1, silicon substrate; 2, Insulator; 3, chemically sensitive membrane; 4, source; 5, drain; 6, insulating encapsulant; 7, analyte solution; 8, reference electrode. [19]





Scheme 1.1. Biocomponent and transducers employed in construction of biosensors.

Transducer	Advantages	Disadvantages	Application
Ion-selective electrode (ISE)	Simple, reliable, easy to transport.	Sluggish response, requires a stable reference electrode, susceptible to	Amino acids, carbohydrates, alcohols and inorganic ions

electronic noise.

Amperometric	Simple, extensive variety of redox reaction for construction of the biosensors, facility for miniaturize.	Low sensitivity, multiple membranes or enzyme can be necessary for selectivity and adequate sensitivity.	Glucose, galactose, lactate, sucrose, aspartame, acetic acid, glycerides, biological oxygen demand, cadaverine, histamine, etc.
FET	Low cost, mass production, stable output, requires very small amount of biological material, monitors several analytes simultaneously.	Temperature sensitive, fabrication of different layer on the gate has not been perfected.	Carbohydrates, carboxylic acids, alcohols and herbicide
Optical	Remote sensing, low cost, miniaturizable, multiple modes: absorbance, reflectance, fluorescence, extensive electromagnetic range can be used.	Interference from ambient light, requires high-energy sources, only applicable to a narrow concentration range, miniaturization can affect the magnitude of the signal.	Carbohydrates, alcohols, pesticide, monitoring process, bacteria and others. . .
Thermal	Versatility, free	No selectivity with	Carbohydrates,

	from optical interferences such as color and turbidity.	the exception of when used in arrangement	sucrose, alcohols, lipids, amines
Piezoelectric	Fast response, simple, stable output, low cost of readout device, no special sample handling, good for gas analysis, possible to arrays sensors.	Low sensitivity in liquid, interference due to non specific binding.	Carbohydrates, vitamins, pathogenic microorganisms (e.g. E. coli, Salmonella, Listeria, Enterobacter), contaminants (e.g. antibiotics, fungicides, pesticides), toxic recognition as bacterial toxins.

Table 1.1. Types of transducers, their characteristics and application.

1.3 Motivation

For the era of minimization requirement of device, the scale of biosensor has become the micro-scale and reached the nano-scale. Because the specific site for immobilization is minimization, discover the ways to improve or amplify the signal is more and more important. The most immediate fashion is to produce more specific sites. The purpose of this thesis is to magnify the specific site for immobilization of bio-molecules.

Further, the selective immobilization of biomolecules onto silicon-based substrates at very high efficiency and reliability is the key to combining biological and electronic elements. In addition, the covalent and non-covalent bonding for capturing electronic signal from biosensor chip which made by semiconductor process are also important technique in the future.

In this work, a reaction template to immobilize biotin is proposed. Then, the biotin

molecule is reacted with streptavidin (SA). The biotin–streptavidin interaction has a very high affinity and therefore represents one of the strongest non-covalent biological interactions. It is frequently used for labeling on various of biomolecules such as antibody, lectins, sugars and nucleics, and has potential applications for biosensors and biosensing arrays. Thus the SA/biotin couple is useful as a molecular linker and has demonstrated extensive applications in biotechnologies such as immunoassays, purification[2,3], and pretargeted diagnosis and therapeutics[4].

1.4 Thesis Organization

This thesis is aimed to study the surface modification and immobilization reaction of biomolecules onto silicon surfaces and to amplify the immobilization site. A new kind of metal-semiconductor-metal (MSM) chip was proposed and used for chemiluminescence-type optical biosensor. The sensor is proposed to detect proteins which were widely used as the target molecule in the medical detection or biological studies. In order to setting up the experimental system, it requires lots of knowledge to accomplish this goal, including nanofabrication technology related to lithography procedures, self-assembly technique, biotechnology, organic chemistry, molecular biology, and electronics. In chapter 1, the general introduce of biosensors is described. Some experimental ideas and techniques from published literatures are cited and discussed in chapter 2. Chapter 3 briefly states the experimental reagents and experimental procedures for this research. In chapter 4, various solid supports were used to immobilize specific protein. We discuss the suitability of support and the activity of immobilized protein. We propose a novel protocol for immobilization and the MSM chip. The new chip is used to detect specific protein was also evaluated. At the last chapter, the conclusions of this thesis are given.

Chapter 2: Literatures Review

In this chapter, we will review some important literatures that relate to the thesis, These literatures cover manipulation, creation and use of materials, devices and systems of chemiluminescence technology, immobilization technique and metal-semiconductor-metal photo diode element which typically have dimension smaller than 100 nm. This is the key spirit of nanotechnology. “There is plenty of room at the bottom,” as Nobel physicist Richard Feynman pointed out more than 40 years ago [1]. Now we continue developing the room by nanotechnology and the succeeding technology.

2.1 Principle of Chemiluminescence Type Biosensor

Based on the spectrum range of the optical biosensor techniques, the main applications at visible wave band are fluorescence emission and chemiluminescence (or bioluminescence). For fluorescence, after absorption of light, the excited species will decay in one of a variety of ways. However, while the excited molecule is undergoing radiationless decay, it may also have time to react with other species, thus transferring its energy to new chemical species and returning to the ground state with a diminished fluorescence output. This process is known as “quenching”, this is a kind of energy transfer, leading the decrease of fluorescence, there are several behaviors happen when fluorescence occurs (shown as Figure 2.1.1):

- (1) $S_1 \rightarrow S_0 + h\nu$ (fluorescence)
- (2) $S_1 \rightarrow S_0$ (internal conversion)
- (3) $S_1 \rightarrow$ triplet states (i.e. T_1) (intersystem crossing)
- (4) $S_1 \rightarrow$ fragments (dissociation)
- (5) $S_1 + Q \rightarrow$ products (quenching)

Chemiluminescence is another type of luminescence which processes low background and high-intensity light output due to the catalyst of enzyme or other catalysts. In contrast, fluorescence requires an external light source as excitation energy which must be filtered to

discriminate the fluorescence signal. The characterization of fluorescence requires the expensive instrument of fluorescence microscopy. Thus limits the sensitivity and the method maybe more complex during the determination. However, chemiluminescence completely eliminates these disadvantages. Chemiluminescence does not require the external light source, and chemiluminescence can be observed by the naked eye. Moreover, it provides real time detection capability. Therefore, chemiluminescence is an excellent way for biochemical detection. Figure 2.1 shows the diagram of fluorescence (a) and chemiluminescence (b); it is obvious at figure 2.1 (a) that fluorescence method needs external light for excitation, chemluminescence is a spontaneous reaction with the emission of light. Ttable 2.1 summarizes the comparison of fluorescence and chemiluminescence method.

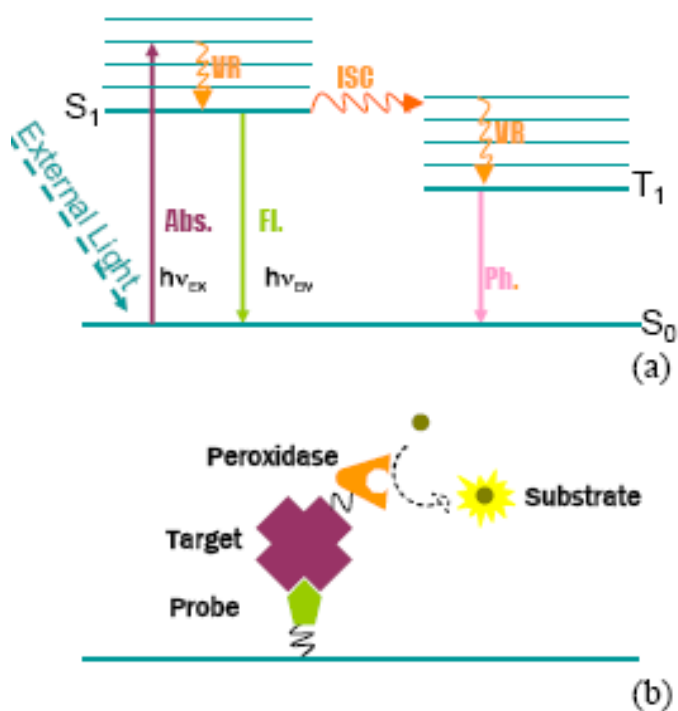


Figure 2.1. (a) A simple Jablonski diagram showing some important radiative and non-radiative process (Abs.: absorption, Fl.: fluorescence, Ph.: phosphorescence, VR: vibrational relaxation, IC: internal conversion, ISC: intersystem crossing) (B) Illustration of chemiluminescence.

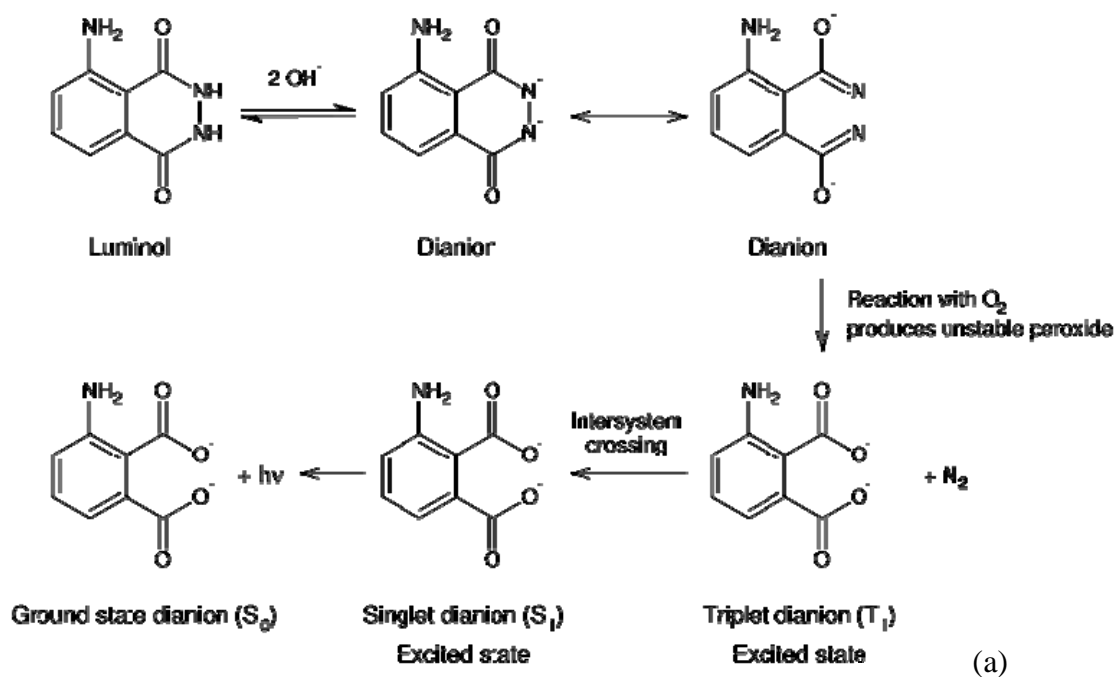
	Fluorescence	Chemiluminescence
Advantages	<ul style="list-style-type: none"> • Sensitive • Variety of fluorescence-conjugated biomolecules available 	<ul style="list-style-type: none"> • No unwanted background luminescence
Disadvantages	<ul style="list-style-type: none"> • Suffering from external light interference • Low photochemical stability • Expensive read out system 	<ul style="list-style-type: none"> • Limited by the availability of chemiluminescent probes

Table 2.1. The comparison between fluorescence and chemiluminescence method.

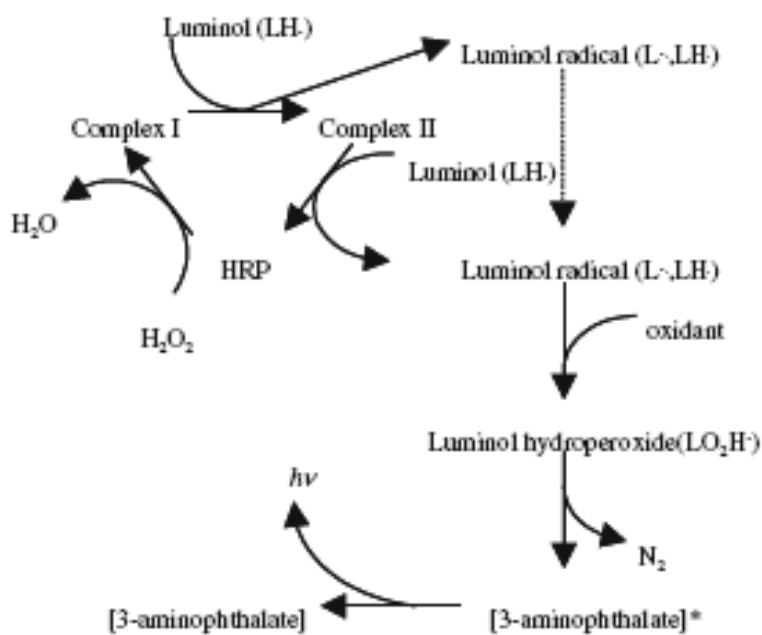
2.1.1 Introduction of Luminol

Luminol is a versatile chemical that exhibits chemiluminescence, with a striking blue glow, when mixed with an appropriate oxidizing agent. It is a white to slightly yellow crystalline solid that is soluble in water and most polar organic solvents.[2]

Luminol is usually used by forensic investigators to detect trace amounts of blood left at crime scenes. It is also used by biologists in cellular assays for the detection of copper, iron, and cyanides. To exhibit its luminescence, the luminol must first be activated with an oxidant. Usually, a solution of hydrogen peroxide (H₂O₂) and a hydroxide salt in water is used as the activator. In the presence of a catalyst such as an iron compound, the hydrogen peroxide is decomposed to form oxygen and water. Figure 2.2(a) demonstrates the typical chemical reaction of luminol.



(a)



(b)

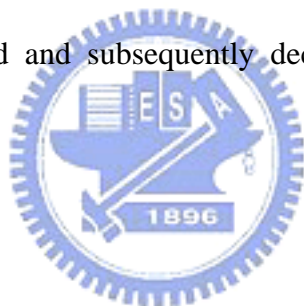
Figure 2.2. (a) The typical reaction of luminol. [3]; (b) the detailed reaction steps of luminol catalyzed by HRP.

2.1.1 Principles of Enzyme Activated Chemiluminescence

HRP (Horse Radish peroxidase, HRP) is one of the most important and one of the smallest enzymes (mol. Wt. ~44kDa) used as a label purpose. The reason for wide application of HRP

as a label is that, in presence of a small amount of enhancers, the intensity of the light emission is increased by several orders of magnitude and background light emission from the luminol-peroxide reagent is greatly reduced, which leads to a dramatic increase in the signal. Luminol is a known substrate, and is used to measure the activity of enzyme [4]. The detailed reaction of HRP enzyme on the luminol molecule is illustrated in figure 2.2 (b).

Detection by chemiluminescence has now become the main method of choice for fast and sensitive assays of enzyme conjugates on blots. While phosphate-containing dioxetane compounds are widely used as the chemiluminescent substrates for alkaline phosphatase conjugates, the compound luminol and its derivatives (diacylhydrazides) are the chemiluminescent substrates of choice for horse radish peroxidase (HRP) conjugates. HRP catalyzes the oxidation of luminol in the presence of hydrogen peroxide, during which an excited intermediate is formed and subsequently decays to the ground state by emitting light[5].



2.2 Immobilization Technique

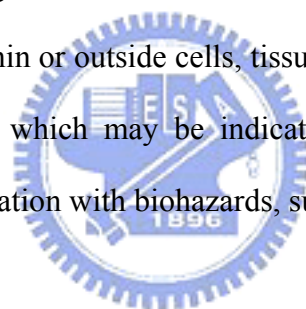
A major advance in materials fabrication technology during the last 10 years has been the development for self-assembly methods [6]. Self assembled monolayers (SAMs) provide well defined structures and chemistries that can be systematically varied. Also, spatially defined arrays of SAMs can be prepared by combining self-assembly with patterning methods such as microcontact printing or photolithography [7]. In addition, SAMs can be used to immobilize peptides, proteins, and other biomolecules to the surface of interest to prepare the complex surfaces required for well-defined biological experiments. A surface skill used in nature with elegance and precision is the ability to order and organize complex molecules at surfaces. Precision immobilization typically aims to copy nature's way of organizing molecules and is thus an example of a biomimetic strategy. Possibilities for surface immobilization of biomolecules are suggested in Table 2.1. The characteristics of successful precision engineered biorecognition surfaces include the presence of one receptor site, an appropriate surface density of those sites, controlled orientation of the sites, some molecular mobility to enhance "docking," and stability (of the biomolecular conformation and the film integrity). The ability to inhibit non-specific reactions (in particular, protein adsorption) is also essential to succeed at emulating nature's surface signal delivery strategy.

Table 2.1: Methods to immobilize active biomolecules onto surfaces [8]

Method	Comment
Non-specific adsorption	Little control is afforded of protein orientation or activity; low durability
Non-specific covalent immobilization	Little control is afforded of protein orientation or activity
Immobilization on an antibody surface	Using monoclonal antibodies, protein orientation can be controlled
HIS tags	Histidine sequences (HIS tags) can be specifically engineered into proteins for attachment and orientation
Biotin/streptavidin	A flexible strategy for tightly fixing protein to surfaces; in vivo biological reaction to streptavidin is a concern
Crystallized protein layers	Useful only in limited cases
Immobilization to a template structure	An evolving field
Biomimetic recognition sites	An evolving field
Incorporation in a supported bilayer	As an emulation of the cell membrane this has the possibility to stabilize fragile proteins
Nucleotide conjugation/hybridization	Many possibilities are being explored
Electrostatic	A non-specific approach to immobilizing proteins when the protein has an isoelectric point higher or lower than seven and a surface has a positive or negative charge

The scientific roots of this area of surface molecule immobilization lie in the Langmuir–Blodgett deposition of lipids and surfactants [9]. The discovery in 1983 of thiol assembly on gold [10] launched an explosion of publications and new discoveries for self-assembling. Self-assembly of complex organic structures on solid surfaces has been observed for phospholipids [11], silanes [12], n-alkyl thiols [13, 14], porphyrins [15], nucleotide bases [16], hydrocarbons [17], proteins [18], and many other organic structures. The choice of a suitable immobilization method is mainly determined by the chemical and physicochemical properties of the immobilization support and of the compound to be immobilized. The adsorption of compounds onto a surface is the simplest immobilization method. It is based on the interactions between local dipoles existing on the interacting molecules. The polarity of the molecule can be stationary due to polar groups, of which $-OH$, $-NH_2$, $-C=O$, NH -groups are of particular importance, as they form strong hydrogen bonds. Most frequently biomolecules are bound covalently to the immobilization support through amino groups, which are accessible on the exposed areas of the biomolecules. They react readily with aldehyde and epoxide groups and with carboxylic or amino groups after activation by carbodiimide- or succinimide-derivatives. Taking protein as an example, after deposition of the protein solution, an incubation step at room temperature in a humid chamber is sufficient for efficient protein immobilization. This makes these procedures compatible with the fabrication of semiconductor devices. Silanisation is the most common procedure for the chemical modification of glass surfaces. Amino groups are introduced by aminopropyltriethoxy- (or trimethoxy) silane. Epoxide groups are introduced via 3-glycidoxypropyltrimethoxysilane. Treatment with periodic acid leads to their oxidation to aldehyde groups. Surfaces with aldehyde or epoxide groups sometimes show reduced background signals, as no unspecific electrostatic interactions are possible, whereas aminofunctionalized surfaces are usually positively charged leading to the unspecific adsorption of negatively charged proteins [19]. Carboxylic groups are present on the surface

of carbonaceous electrodes or are generated on the surface of gold layers by self-assembling of thiol compounds, such as 11-mercaptopundecanoic acid [20]. These groups have to be activated to allow covalent coupling of proteins, which is done by incubation with a carbodiimide, such as 1-ethyl-3-(3-dimethylaminopropyl) carbodiimide hydrochloride (EDC) in the presence of N-hydroxysuccinimide (NHS). Proteins with an extremely high affinity for biotin are avidin and streptavidin (dissociation constants of approx. 10^{-15} M). Due to the four biotin-binding sites on each protein molecule a layered structure can be built with a biotinylated surface, a biotin binding protein in the second layer and the 16 biotinylated capture protein [19]. Protein-sensing devices are of increasing importance in the fields of diagnosis, monitoring systems or biological research, as it is realized that proteins are one of the active compounds in organisms. Thus their concentrations, covalent modifications, localizations and activities within or outside cells, tissues or organisms reflect reactions of the organism to its surroundings, which may be indicative of diseased states, toxic or other adverse effects or for contamination with biohazards, such as microbial toxins.

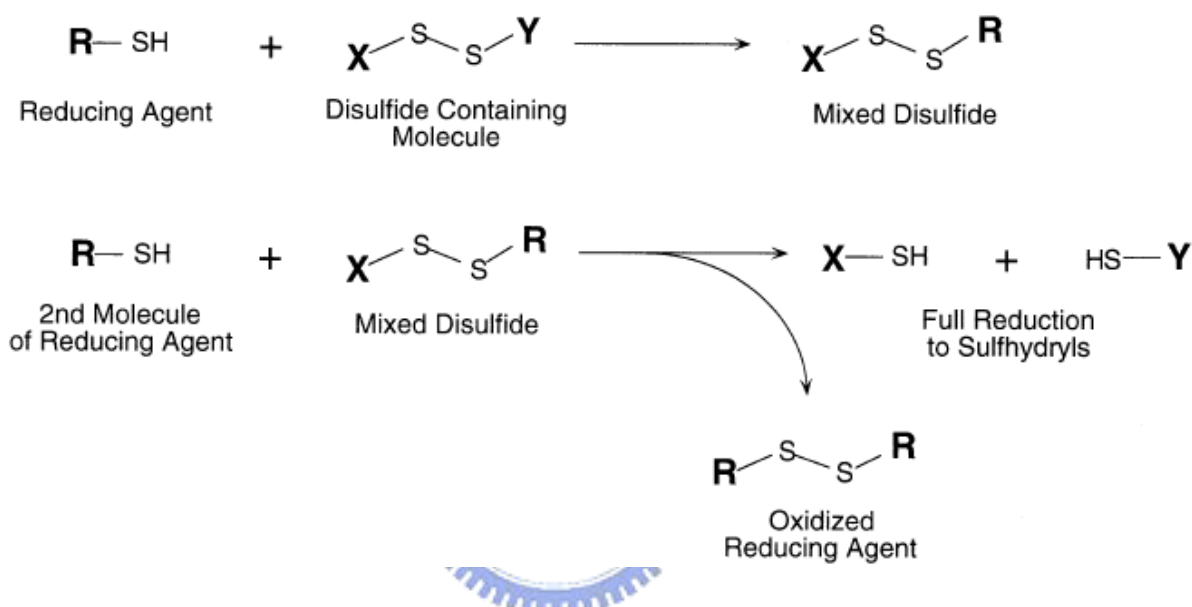


2.2.1 Cleland's reagent: DTT

Dithiothreitol (DTT) is a Cleland's reagent; the reducing potential of this versatile reagent was first described by Cleland in 1964. Due to their low redox potential (-0.33V) they are able to reduce virtually all accessible biological disulfides and maintain free thiols in solution despite the presence of oxygen. The compounds are fully water-soluble with very little of the offensive odor of the 2-mercaptoethanol they were meant to replace. Since Cleland's original report, literally hundreds of references have appeared citing the use of mainly DTT for the reduction of cystine and other forms of disulfides.

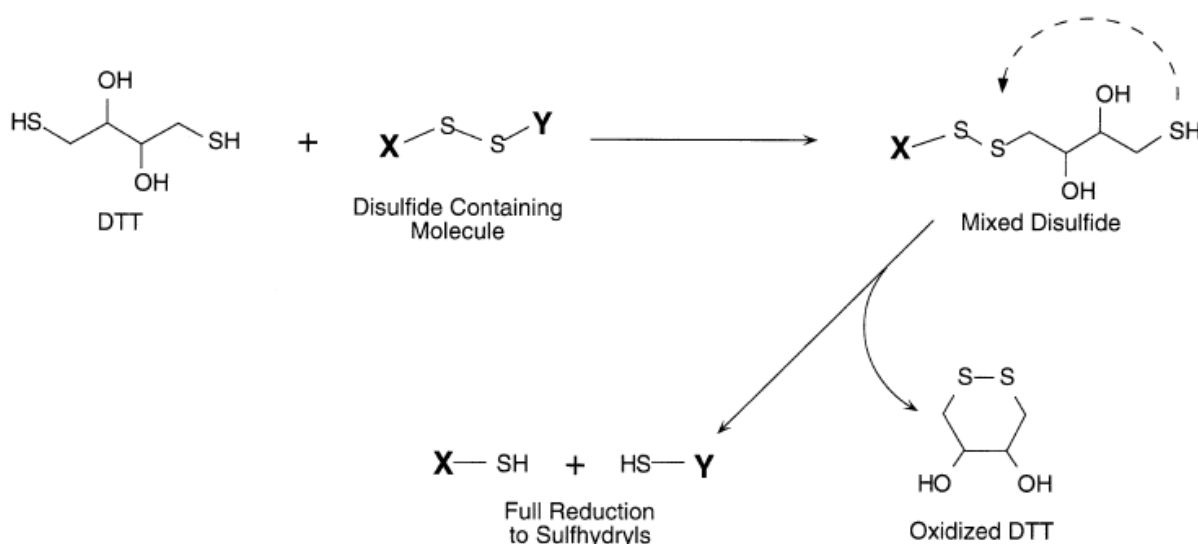
The unique characteristics of DTT is mainly reflected in their ability to form intramolecular ring structures upon oxidation. Disulfide reductants such as 2-mercaptoethanol, 2-mercaptoethylamine, glutathione, thioglycolate, and 2,3-dimercaptopropanol cleave

disulfide bonds in a two-step reaction that involves the formation of a mixed disulfide (Scheme 2.1 and Scheme 2.2). In the second stage of the reducing process, the mixed disulfide is cleaned by another molecular of reductant, freeing the sulfhydryl and forming a dimer of the reducing agent through the formation of an intermolecular disulfide exchange is nearly equivalent for the reductant and target protein. Thus, monothiol compounds are usually require in extreme excess to drive the reaction to completion [21].



Scheme 2.1. Thiol-containing disulfide reductants reduce disulfide groups through a multistep process producing a mixed intermediate [21].

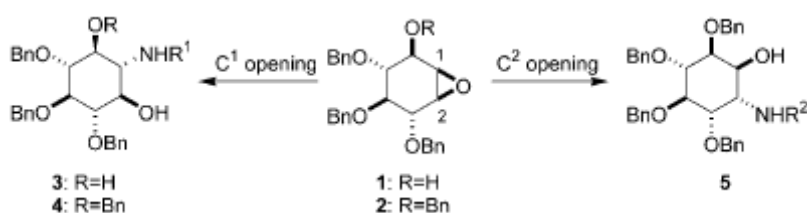
The presence of two sulfhydryl group in DTT, however, allows the formation of a favored cyclic disulfide during the course of target protein reduction (Scheme 2.2) This drives the equilibrium toward the reduction of target disulfides. Therefore, complete reduction is possible with much lower concentrations of DTT than when using monothiol systems.



Scheme 2.2. DTT is highly efficient at reducing disulfides, since a single molecule can reduce the intermediate mixed disulfide by forming a ring structure [21].

2.2.2 The Effect of Li as a Chelating Agent on the Ring Opening of Cyclitol Epoxides

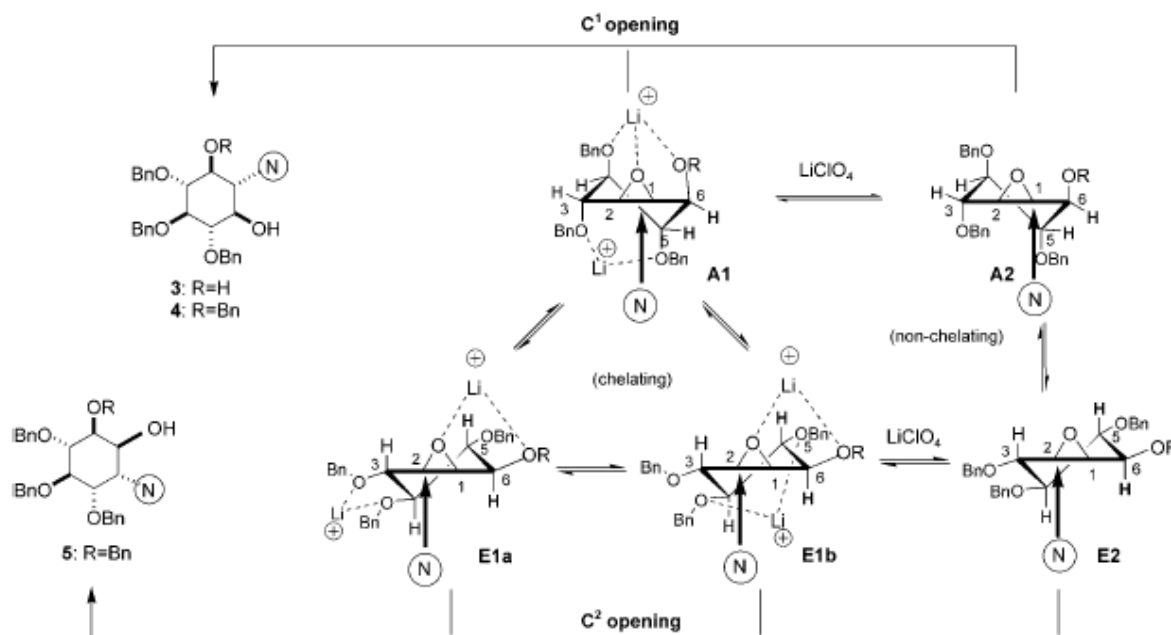
Over the last years, aminocyclitols have gained interest as pharmacological tools for the study of cellular processes linked to the inositol phosphate cycle, as well as potential glycosidase inhibitors [22, 23]. The regio- and stereoselective synthesis of aminocyclitol is more and more interesting [24]. Pedro Serrano et. al have demonstrated a useful ring opening process for epoxides (in Scheme 2.3)



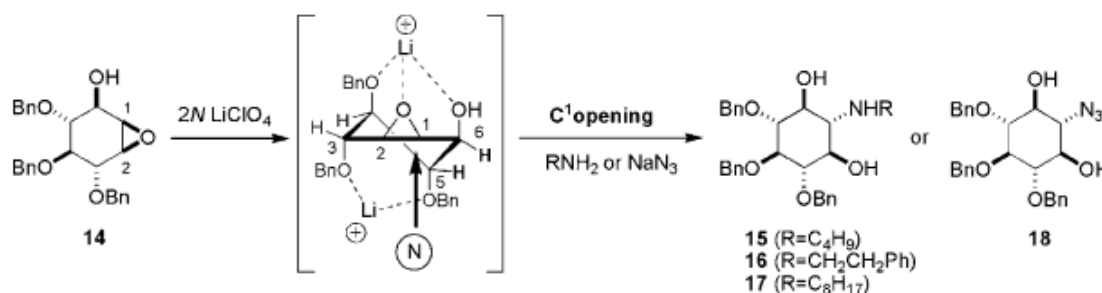
Scheme 2.3. Regio- and stereocontrolled opening of cyclitol epoxides.[34]

Epoxide opening is well documented in the literature,[25] particularly Li salts, to promote a complete regiochemical epoxide opening.[26] Thus, in the presence of LiClO_4 , the conformational equilibrium in the cis isomer is shifted towards a reactive conformation in

which the benzyloxy group adopts an axial disposition to enable intramolecular metal chelation with the epoxide. Li salts behave similarly to promote epoxide opening through an intramolecular chelation process. The Scheme 2.4 and Scheme 2.5 demonstrate the main reaction flow of ring opening reaction for epoxides.



Scheme 2.4. Lithium promoted opening of cyclitol epoxides 1 (R=H) and 2 (R=Bn). [26]



Scheme 2.5. Synthesis of cyclitol analogues by regioselective C1 opening of the starting epoxide. [27]

2.4 Fundamentals of the MSM-PD

The MSM-PD is a planar device, and it consists of two back-to-back connected Schottky diodes on a semiconductor layer. The metal structure is composed of two contact pads and interdigitated lines, which form the active area of the device. The device works by absorbing optical energy and converting incident photons into a time-varying electrical signal. When the active area of the device is illuminated, carriers in the semiconductor absorption layer (also known as electron-hole pairs) are generated by incident photons having energy greater than the bandgap energy (E_g). The carriers are transported to the metal contact pads, and a current is detected in the external circuit under the application of an external bias voltage. Figure 2.3 shows the cross section of the MSM-PD, signifying the dimensions, carrier motion, and the electric field orientation. S and W refer to the electrode spacing and width, respectively, d to the thickness of the active area, and E to the electric field.

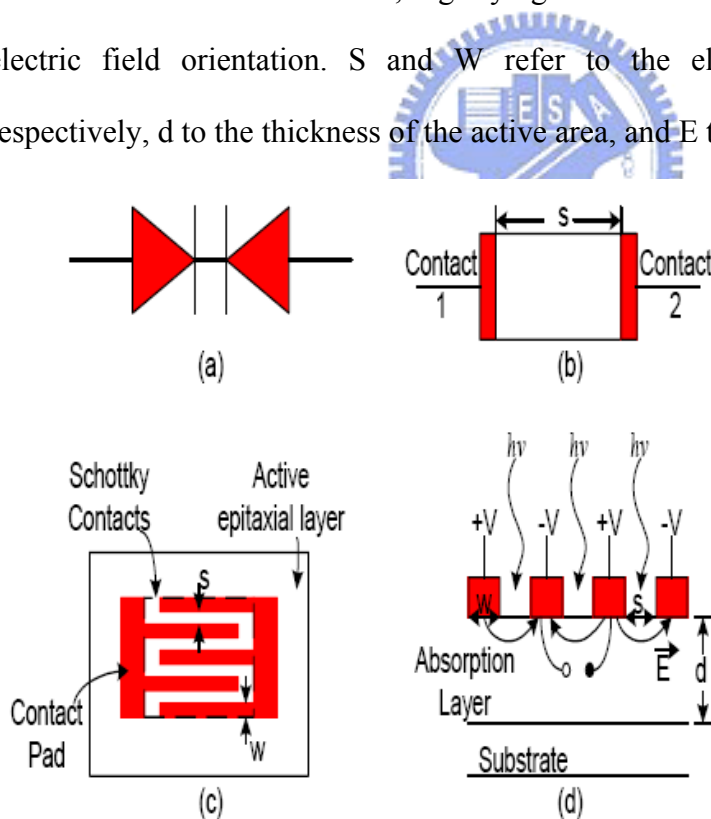


Figure 2.3 (a) schematic symbol, (b) 1-D schematic, (c) top view, and (d) cross-section view.

Figure. 2.4 (a) illustrates a schematic diagram of symmetrical MSM structure with

metal contacts to uniform-doping n-type semiconductor. The charge distribution, electric-field distribution, and energy-band diagrams in this device with a small positive bias voltage are shown in Figure. 2.4 (b), (c), (d), respectively [28]. As a small positive bias voltage is applied, one side is forward-biased and the other one is reverse-biased. The W_1 and W_2 denote the depletion widths at the forward and reverse biased Schottky junctions in the n-type semiconductor, respectively.



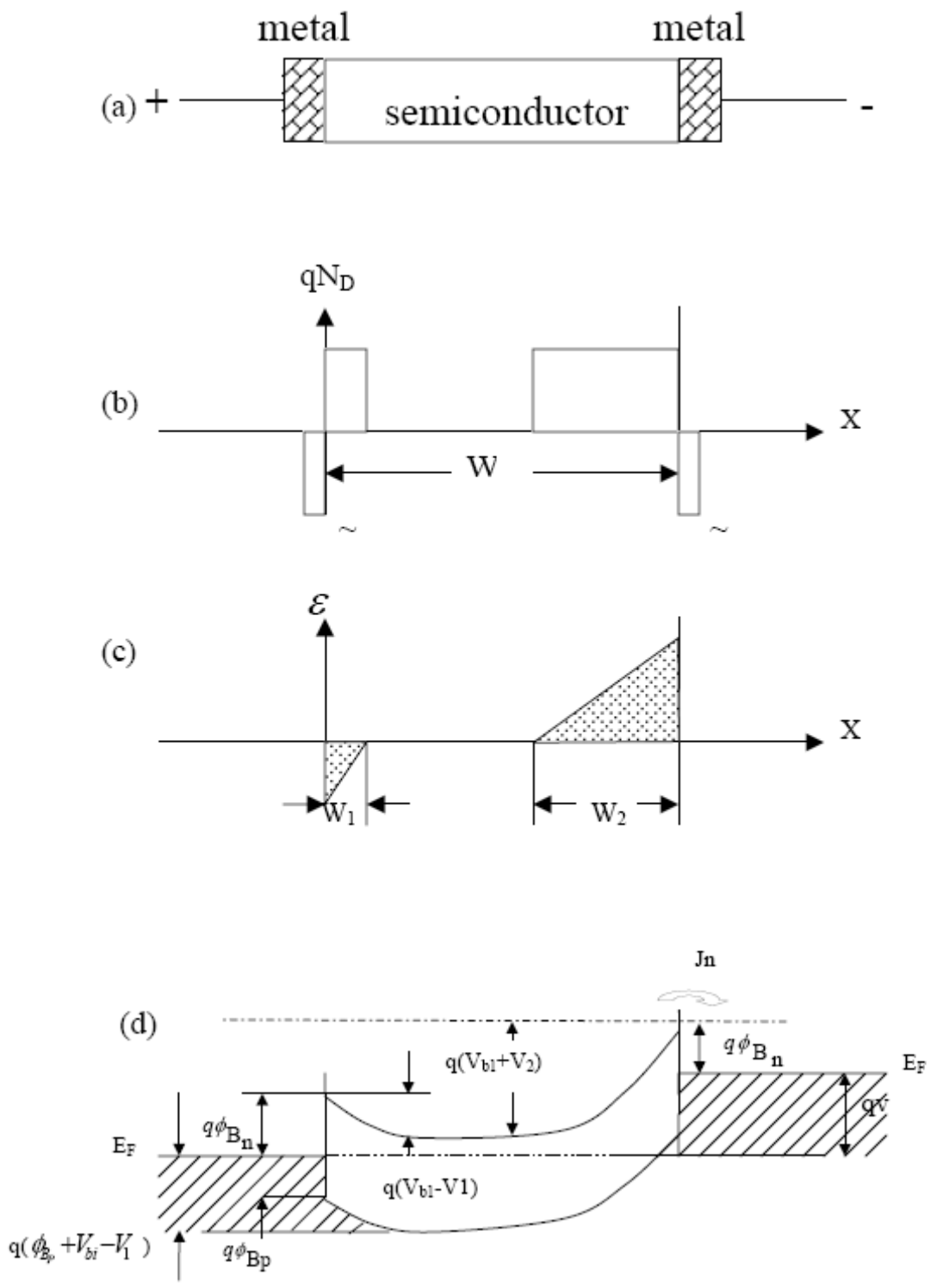


Figure 2.4 (a) schematic diagram of MSM-PD (b) charge distribution under low bias voltage (c) electric field distribution under low bias voltage (d) energy band diagram of MSM-PD

2.2.1 Current Transport Mechanism

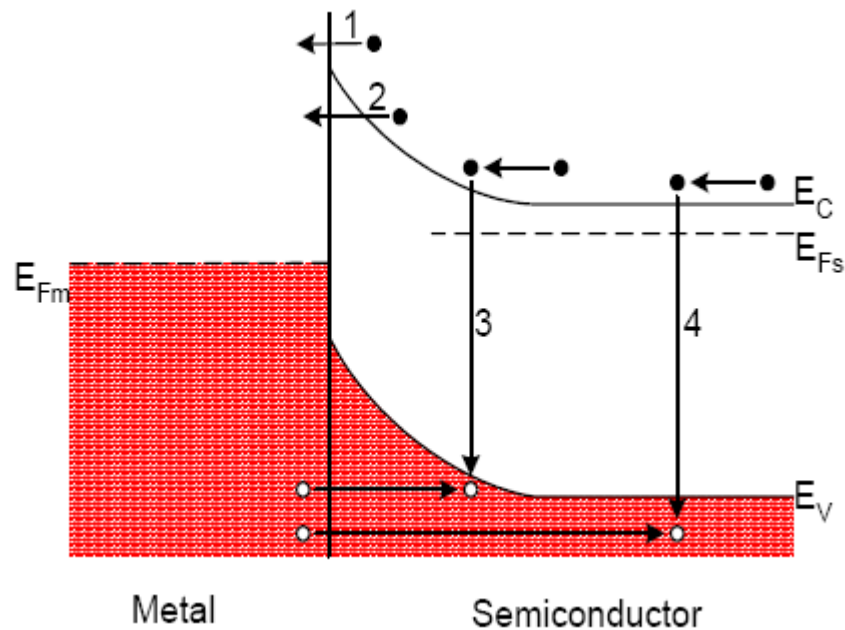


Figure 2.5 Current transport mechanism under forward bias

The current transport in metal-semiconductor contacts is primarily due to majority carriers. The four basic transport processes for a Schottky diode [29, 30, 31] are shown in Figure 2.5 under forward bias conditions (the inverse processes occur under reverse bias):

- (1) Emission of electrons from the semiconductor over the top of the potential barrier into the metal
- (2) Quantum mechanical tunneling of electrons through the barrier
- (3) Recombination in the space-charge region
- (4) Recombination in the neutral region (also hole injection from the metal to the semiconductor)

Condition (1) and (2) are dominant for moderately doped semiconductor, and heavily doped semiconductors, respectively. Diffusion [32, 33], thermionic emission[34], and combined thermionic emission diffusion[35, 36] theories are used to study the emission of electrons over the barrier. The thermionic emission theory

applicable to high-mobility semiconductors; and for low mobility semiconductors the transport is described by the diffusion theory.

2.3 Characteristic parameters of MSM-PD

2.3.1 Quantum efficiency

Quantum efficiency, η ($0 \leq \eta \leq 1$) of a photodetector is defined as the number of carriers (electron-hole pairs) collected to produce the photo current (I_{ph}) generated per the number of incident photons. The equation of external quantum efficiency (η) is given by

$$\eta = \frac{I_{ph}/q}{P_{in}/h\nu}$$

Where q is magnitude of the electronic charge, h is Plank constant, ν is the frequency of incident light.

2.3.2 Responsivity

Responsivity of the detector is the ratio of the photo current flowing in the detector to the incident optical power:

$$R = \frac{I_{ph}}{P_{in}} = \frac{\eta\lambda}{1.24} \text{ (A/W)}$$

Where λ is the wavelength of incident light.

2.3.3 Response time

The response-time limit of all photodetectors is determined by basically three effects: the time of carrier diffusion to the junction depletion region, τ_0 ; the transit time of carrier drift across the depletion region, τ_s ; and the RC time constant associated with circuit parameters including the junction capacitance C and the parallel combination of device resistance and external load.

Chapter 3: Experiments

3.1 Reagents and Instruments

All the experiments were proceeded at either National Chiao Tung University (NCTU) or National Nano Device Laboratories (NDL). All the equipments were also conducted in our laboratories in NCTU. The reagents were purchased commercially and used by following with the directions unless specially mentioned. All the reagents were listed alphabetically in the form of “Name {abbreviation; chemical formula; purity; manufacturer}”. Some information will be omitted if not available or not necessary. The following text will use the abbreviation of the reagent.

3.1.1 Reagents

3-aminopropyltriethoxysilane {APTES; $\text{H}_2\text{N}(\text{CH}_2)_3\text{Si}(\text{OC}_2\text{H}_5)_3$; 97% purity; Sigma}

APTES was used to modify the property of the SiO_2 surface. The ethoxy functional groups of APTES were displaced through formation of covalent bond between the hydrophilic hydroxyl groups of the SiO_2 surface and the silicon atom in APTES molecule. This process leads to the formation of a molecular layer of amino groups for futher bonding with biochemical materials.

Acetone { CH_3COCH_3 ; $\geq 99.5\%$ purity; Sigma}

Acetone was used to remove the excess and unnecessary chemical reagent or particles.

Toluene { $\text{C}_6\text{H}_5\text{CH}_3$; $\geq 99.5\%$ purity, anhydrous; Sigma}

Toluene was diluted with DI water to provide an environment that facilitates the APTES binding to the SiO_2 surface.

Bovine serum albumin {BSA; for molecular biology, powder}

Bovine serum albumin consists approximately 50% of the total protein in serum. It is a non-acetylated protein served as a blocking agent.

Deionized and distilled water {DI water, ddH₂O}

The water we used was purified with filters, reverse osmosis, and deionized system to the resistance more than 18 MΩ · cm. DI water was used to clean, wash, and as a solvent.

***N,N*-Dimethylformamide {DMF; HCON(CH₃)₂; for molecular biology, ≥99% ; Sigma}**

It was a solvent for dissolving many hydrophobic organic compounds like rhodamine in the experiments.

Hydrogen chloride {HCl; ≥99% purity; Sigma}

1 M HCl in DI water was used for pH adjustment.



Hydrogen peroxide {H₂O₂; ≥30% purity; Sigma}

Hydrogen peroxide was mixed with sulfuric acid to form piranha solution which cleaned the wafer surface.

Phosphate-buffered saline tablets {PBS, 1X; CALBIOCHEM}

PBS, a biological buffer solution, was used to increase the selectivity of the DNA chips by washing away any non-hybridized nucleic acids. This chemical is dissolved in one liter ddH₂O to yield 10 mM phosphate buffer, pH 7.4, 140 mM NaCl, 3 mM KCl.

Rhodamine B amine {C₂₈H₃₁N₃O₃; Sigma}

This chemical possessed fluorescent property and was reacted to the functional group of

aldehyde. It was very light-sensitive and must be stored at 4°C. During the processing, it must keep from light with aluminum foil.

Sodium chloride {NaCl; ≥ 99.5%; Sigma}

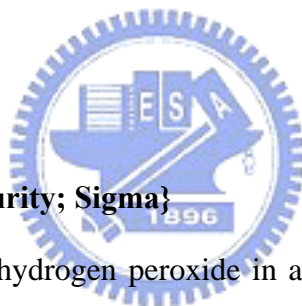
Sodium chloride was used to prepare SSC or other biological buffer.

Sodium hydroxide {NaOH; 98% purity; Sigma}

10 M Sodium hydroxide in DI water was used to adjust the pH.

Sodium phosphate dibasic dihydrate {NaH₂PO₄; ≥99.5%; Riedel-deHaën}

Sodium phosphate solution was a widely used biological buffer. This chemical was also a family of PBS.



Sulfuric acid {H₂SO₄; 98% purity; Sigma}

Sulfuric acid was mixed with hydrogen peroxide in a 3:1 ratio to remove impurities on the surface of the wafer or devices. This material was very corrosive and dangerous. We must handle it with carefullness and patience.

Tween 20 {Polyethylene glycol sorbitan monolaurate; Sigma}

Tween 20 was a non-ionic detergent to control the stringency of hybridization.

Cysteamine {NH₂ CH₂ CH₂SH; ~95%; Sigma}

Cysteamine was used for chemical modification.

DDT (Dithiothreitol) {C₄ H₁₂ O₂ S₂; >99%; DUCHEFA BIOCHEMIE}

This reagent is used as Cleland's reagent.

Sulfo-NHS-Biotin { C₁₄H₁₈O₈N₃S₂Na; 443.43; Pierce}

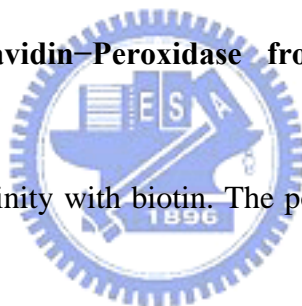
The reagent is used for labeling surface functional groups and biologically active molecules such as antibodies, lectins sugars, nucleic acids or molecules with free amino group. Stored under 4°C.

Streptavidin–FITC from *Streptomyces avidinii* {essentially salt-free, lyophilized powder, ≥ 5 units/ mg protein; Sigma}

This protein had a high affinity for biotin. Prior to use, the powder needed to dissolve in the PBS. It must be stored under -20°C.

Streptavidin-HRP { Streptavidin–Peroxidase from *Streptomyces avidinii*; 443.43; Sigma}

This protein exhibited high affinity with biotin. The powder needs to dissolve in PBS buffer prior to use. Stored under -20°C



Luminol {from Chemiluminescent Peroxidase Substrate; Sigma}

The kit for chemiluminescence was consisted with luminol and H₂O₂.

Conduritol B epoxide {1,2-Anhydro-myo-inositol; 155.68, Sigma}

This reagent is used for surface immobilization.

3.1.2 Instruments

Photo Diode

Operated at 1V reverse-biased, 1mA = 100mW/cm², only 300 ~ 800 nm wavelength can be emitted from the diode.

Fluorescence Microscopy

Olympus BX21 with microscope digital camera of DP71.

Image Analysis Software

Image-Pro Plus Version 6.0, Media Cybernetics Inc.

UV-Visible Spectrophotometer

SHIMADZU, UV-1601

Semiconductor Parameter Analyzer

HP-4156 C, Agilent.



3.2 Procedures

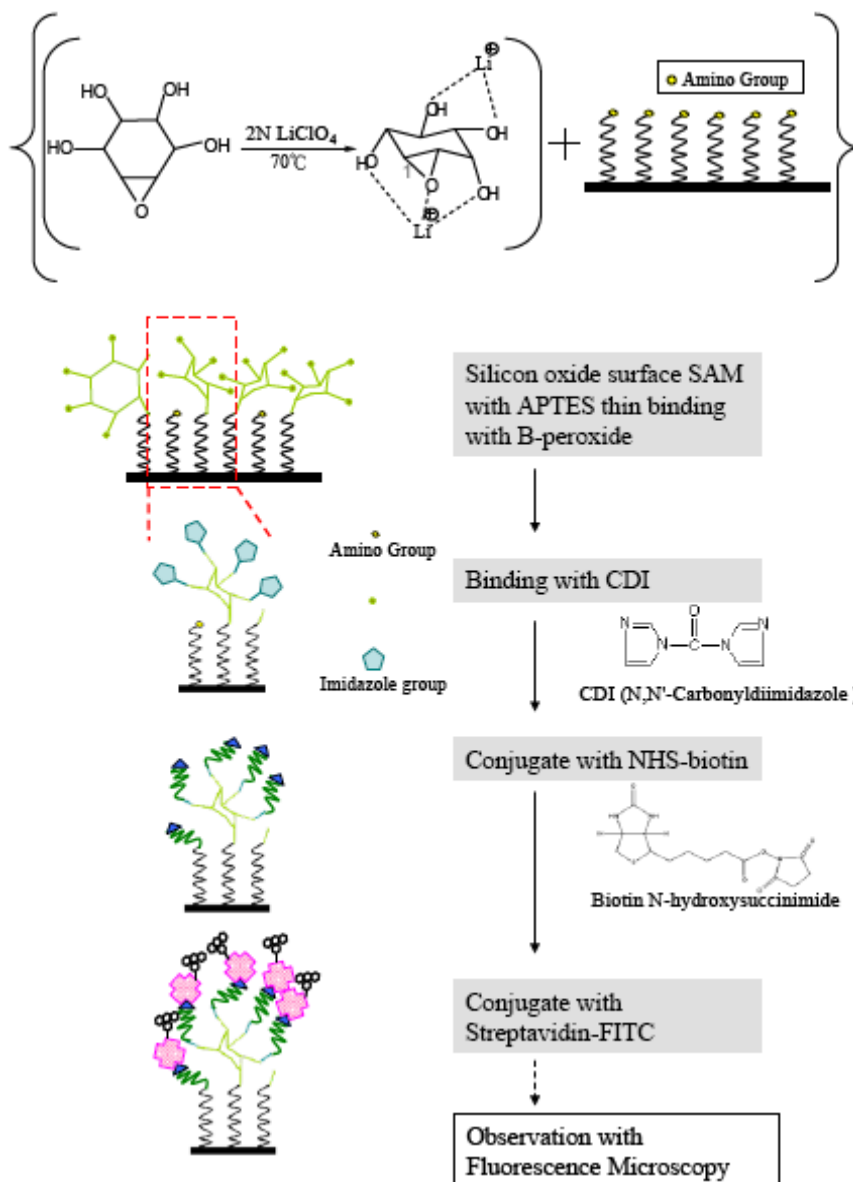
The deionized water (DI water) with 18 M Ω -cm was used in the thesis. A thermal oxide layer was grown on <100> silicon wafers by heating to 900°C for 3 hours.

3.2.1 Self-assembly of B-epoxide on APTES for enhancing immobilization efficiency of streptavidin

- Step 1: Cleaning the silicon wafer with piranha solution. Prior to any functionalization, the chip surface was cleaned in piranha solution (H₂SO₄ : H₂O₂ = 7 : 3) for 1 hour. To prepare the piranha solution, first pouring H₂SO₄ and then adding H₂O₂, check the temperature to avoid too much increase since it will extreme hot and dangerous.
- Step 2: The slides are then washed thoroughly with DI water and then dry the slides by flushing nitrogen. After that, soaked slides with 10% APTES in dried toluene for 30 minutes at room temperature.
- Step 3: Preparing the 10mM B epoxide solution (solvent: H₂O), adding equal volume of LiClO₄ solution with concentration of 20mM.
- Step 4: Removal of the solution of APTES, the microchips were rinsed several times with toluene and acetone and dried in an oven at 120 °C for 1 hour.
- Step 5: Removing the slides away the oven, waiting a moment until the temperature of slides return to room temperature. Soaking the slides with LiClO₄ solution at 70 °C for 12 hours.
- Step 6: Removing the slides and rinsing with DI water, then soaking the slides with 5mM sulfo NHS-biotin (solvent: DMSO).
- Step 7: Removing the slides and rinsing with PBS buffer solution with 0.3% Tween 20, then soaking the slides with BSA solution for 20 minutes.
- Step 8: Removing the slides and rinsing with DI water, then soaking the slides with 5mM

sulfo NHS-biotin (solvent: DMSO) for 6 hours.

- Step 9: Removing the slides and rinsing with PBS buffer solution, then soaking with streptavidin-FITC solution (0.01mg streptavidin-FITC with 10ml PBS buffer) for 2hours.



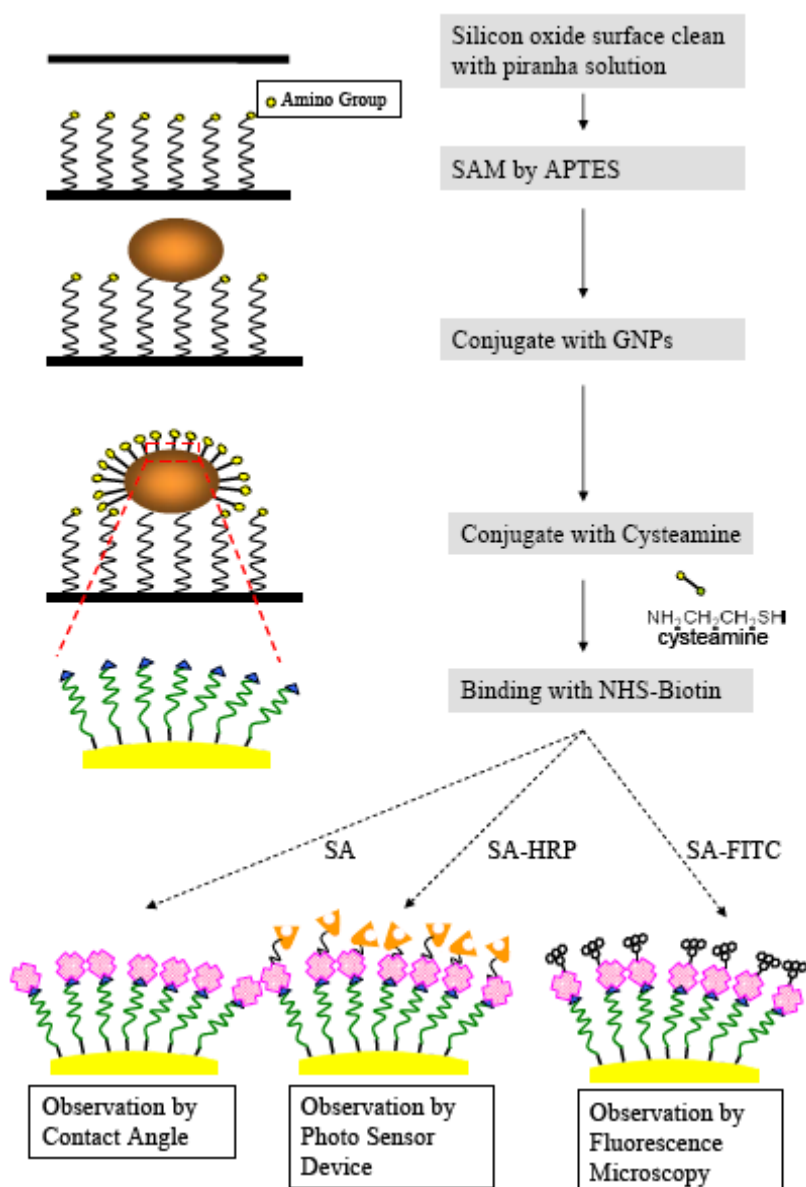
Scheme 3.1. The procedures for the of immobilization of biotin with streptavidin.

3.2.2 Self-assembling of cysteamine on GNPs for enhancing the immobilization efficiency of streptavidin

- Step 1: Cleaning the silicon wafer with piranha solution. Prior to any functionalization, the chip surface was cleaned in piranha solution ($\text{H}_2\text{SO}_4 : \text{H}_2\text{O}_2$, 7 : 3) for 1 hour. To prepare

the piranha solution first, pouring H_2SO_4 and then adding H_2O_2 , check the temperature to avoid too much increase since it will extreme hot and dangerous.

- Step 2: The slides are then washed thoroughly with DI water and then dry the slides by flushing nitrogen. After that, soaked slides with 10% APTES in dried toluene for 30 minutes at room temperature.
- Step 3: Removial of the solution of APTES, the microchips were rinsed several times with toluene and acetone and dried in an oven at $120\text{ }^\circ\text{C}$ for 1 hour.
- Step 4: Removing the slides away the oven, waiting a moment until the temperature of slides return to room temperature. Soaking slides with GNPs solution at RT for 30 minutes, slides are then washed with deionised water.
- Step 5: Then preparing the cysteamine solution, 10ml deionised water with 0.0154g cysteamine and 0.0154g DDT, after thoroughly mixing and dissolving, GNPs-APTES-modified slides were dipped into this solution for 3 hours.
- Step 6: Removing the slides and rinsing with DI water, then soaking the slides with 5mM sulfo NHS-biotin (solvent: DMSO) for 6 hours.
- Step 7: Removing the slides and rinsing with PBS buffer solution, then soaking with streptavidin-FITC solution (0.01mg streptavidin-FITC with 10ml PBS buffer) for 2hours, streptavidin-FITC can be substituted by streptavidin or streptavidin-HRP.



Scheme 3.2. The procedures for the immobilization of biotin with streptavidin by the assisting of GNPs and cysteamine

3.2.3 Chemiluminescence type photo-sensor from luminol reaction of HRP-catalyst

In this part, we fabricated MSM (metal-semiconductor-metal) chip by a serie of semiconductor processes, then we self-assembled and immobilized several molecules onto the surface of MSM chip. Finally, we poured the substrate of chemiluminescence into the system and recorded captured the electronic signal by precision instrument.

3.2.3.1 MSM Biosensor Manufacturing

Single-crystalline N-type $\langle 100 \rangle$ silicon wafers (resistance: $2\sim 7\Omega\text{-cm}$) were used through all the experiments.

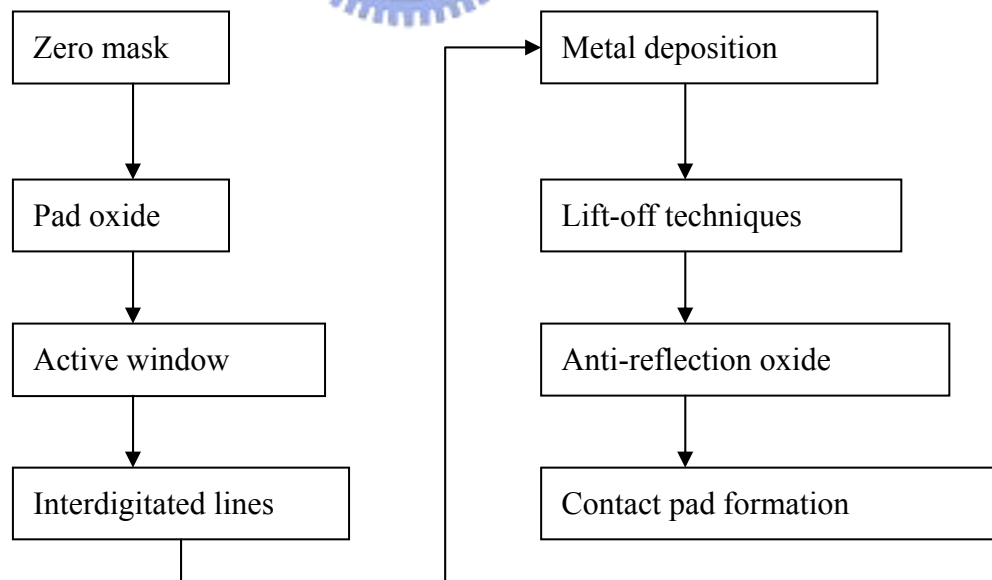
The detailed processes of Metal-Semiconductor-Metal Photodetector are listed below.

Fabrication process :

- Step 1: Standard cleaning [48] the silicon wafer. Firstly, using the DHF to remove the native oxide on the silicon surface. Secondly, rinsing the wafers in SC-1 solution to remove particles and some organic compounds, then rinsing the wafers in SC-2 solution to remove alkaline metallic ions and alkaline-earth metallic ions. Since H_2O_2 was added in SC-1 and SC-2 to improve the activity of the chemical, the oxidative activation of H_2O_2 will result in the formation of native oxide. Finally, rinsing the wafers in DHF solution to remove the native oxide film.
- Step 2: Send the wafers into low pressure furnace tube to grow 2000 \AA thermal oxide.
- Step 3: Spin coating E-beam positive photoresist on the wafers.
- Step 4: Using E-beam lithography (Leica WePrint 200) to write the zero mask pattern on the wafers. (The zero-mask is served as alignment calibration.) the wafers were developed in TRACK (TEL CLEAN TRACK MK-8) system. 2.38% tetramethyl ammonium hydroxide (TMAH) solution was used for the development.
- Step 5: Etching away the oxide layer by reactive-ion-etching (RIE) [49] (TEL5000).
- Step 6: Removing the photoresist by OZONE plasma (FUSION OZONE ASHER) and then rinsing in SPM solution ($\text{H}_2\text{SO}_4 : \text{H}_2\text{O}_2 = 3 : 1, 120^\circ\text{C}$). Then immersion in SC-1 to remove side-wall polymers formed during step 5.
- Step 7: Etch the silicon layer by TCP. Zero mask patterns are finished here.
- Step 8: Depositing 350 \AA thermal oxide (DRY OX) by low pressure horizontal furnace tube.
- Step 9: Spin coating E-beam resist, then patterning the active window by E-beam

lithography.

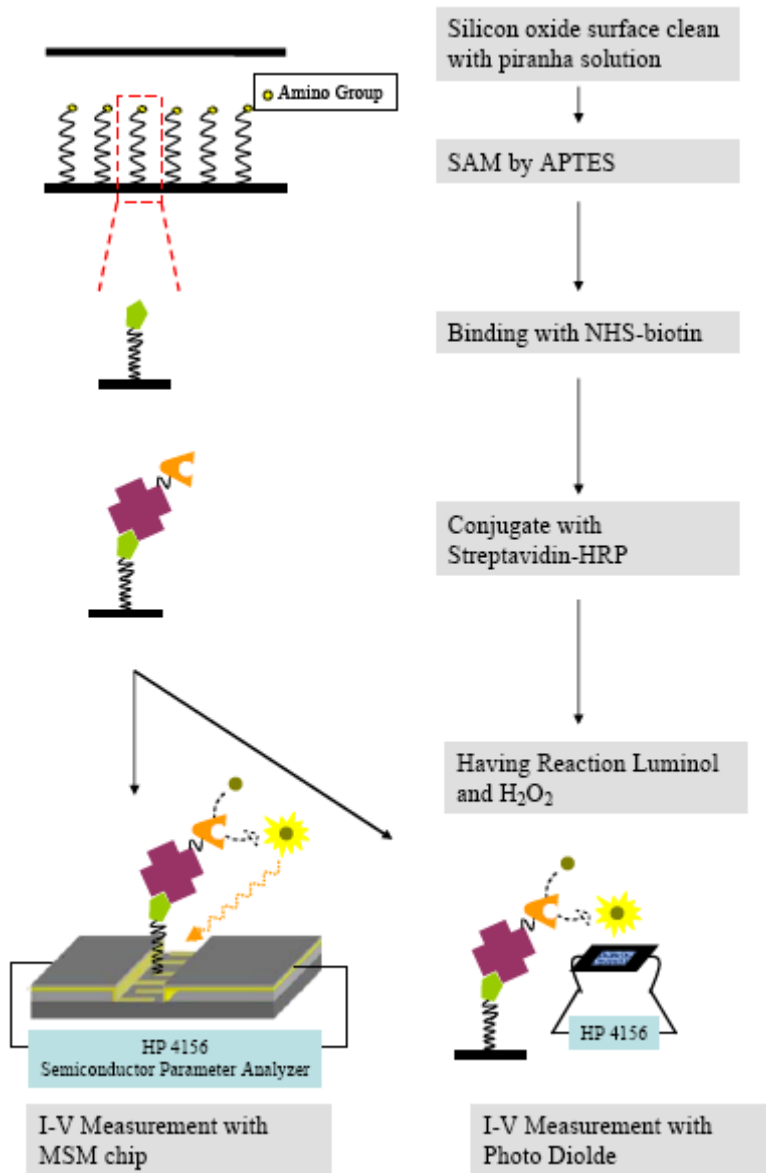
- Step 10: Etching away dry oxide layer by TEL5000. Then rinsing in SC-1 to remove side-wall polymer.
- Step 11: Removing photoresist by OZONE and SPM.
- Step 12: Spin coating photoresist and then patterning interdigitated lines by E-beam lithography. Develop by TRACK system.
- Step 13: Using TCP to etch away the single crystalline silicon and ensuring the better adhesion and contact of metal lines with the silicon surface.
- Step 14: Depositing metals by thermal coater (Cr,Au) or Electron-Gun (Cr,Pt).
- Step 15: Using lift-off techniques to remove the unwanted metal.
- Step 16: Depositing oxide passivation layer by PECVD. The thickness is 760Å.
- Step 17: Spin coating E-beam photoresist then E-beam lithography to form the pattern of probe contacts. Then, development by TRACK and etch away by BOE (Buffered oxide etching solution $\text{NF}_4 : \text{HF} = 5:1$) The device is completely finished here.



Scheme 3.3. Process flow chart of MSM-PD fabrication.

3.2.3.2 Immobilization of Biomolecules onto the Surface on MSM Biosensor

- Step 1: Cleaning the silicon wafer with piranha solution. Prior to any functionalization, the chip surface was cleaned in piranha solution ($\text{H}_2\text{SO}_4 : \text{H}_2\text{O}_2 = 7 : 3$) for 1 hour. To prepare the piranha solution first, pour H_2SO_4 and then adding H_2O_2 , check the temperature to avoid too much increase since it will extremely hot and dangerous.
- Step 2: The slides are then washed thoroughly with DI water and then dry the slides by flushing nitrogen. After that, soaked slides with 10% APTES in dried toluene for 30 minutes at room temperature.
- Step 3: Removal of the solution of APTES, the microchips were rinsed several times with toluene and acetone and dried in an oven at $120\text{ }^\circ\text{C}$ for 1 hour.
- Step 4: Removing the slides away the oven, waiting a moment until the temperature of slides return to room temperature.
- Step 5: Removing the slides and rinsing with DI water, then soaking the slides with 5mM sulfo NHS-biotin (solvent: DMSO) for 6 hours.
- Step 6: Removing the slides and rinsing with PBS buffer solution, then immersion with streptavidin-HRP solution (0.01mg streptavidin-FITC with 10ml PBS buffer) for 2hours.



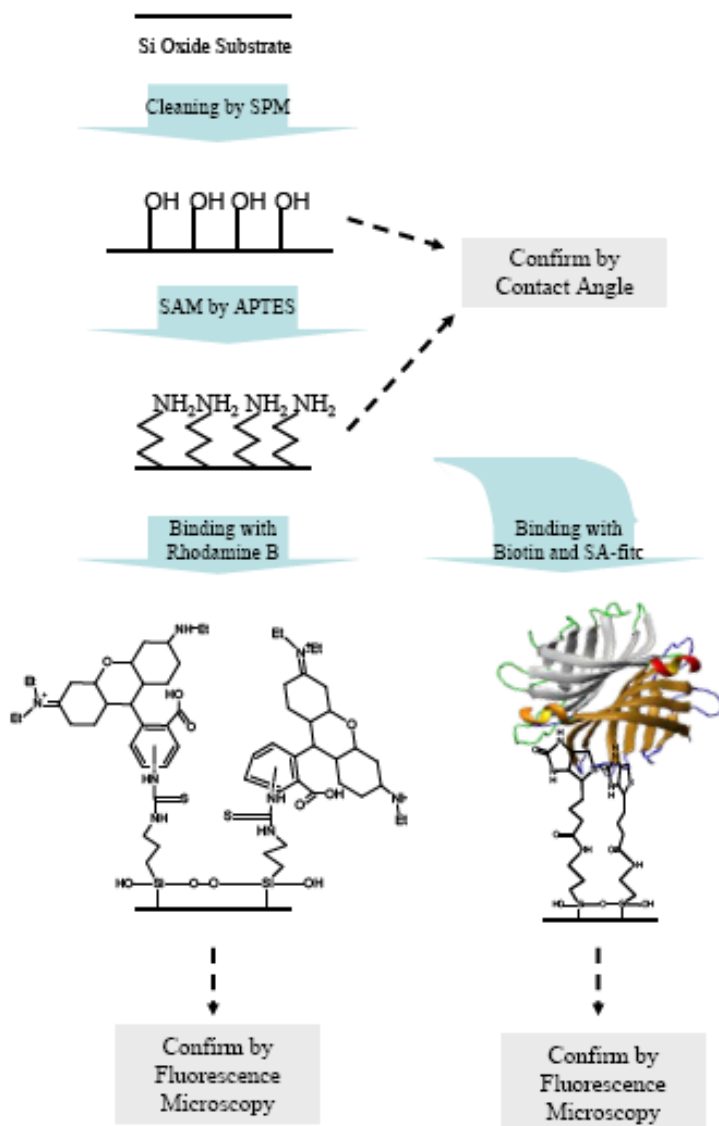
Scheme 3.4. Diagram of MSM photo sensor or photodiode with chemiluminescence reaction.

Chapter 4: Results and Discussion

We studied the suitable molecules for immobilization and metal nanoparticles on silicon dioxide surface. By utilizing semiconductor process, we immobilized appropriate molecules on selected area of pattern surface with self-assembling technique. After that, we successfully immobilized GNPs (gold nanoparticles) on the selected area. Furthermore, we also grafted the other molecules onto GNPs. By following this protocol procedure, we had attached a couple of biomolecules. We evaluated the immobilization efficiency with SEM, fluorescence microscopy, UV-visible spectrophotometer and IV characteristics.

4.1 Optimization of Self-assembly Parameters on Silicon Oxide Surface

The contact angle is the angle at which an equilibrium is reached between solid, liquid and gas phases. The contact angle is specific for any given system and is determined by the interactions across the three interfaces. This technique is usually performed with a small liquid droplet resting on a flat horizontal solid surface. The shape of the droplet can be determined by the Young-Laplace equation. The contact angle plays the role of a boundary condition. Contact angle is measured by a contact angle goniometer. The contact angle is not limited to a liquid/vapor interface; it can be also applied to the interface of two liquids phases or two vapors analogues. In this study, we use DI-water as liquid phase. Figure 4.1(a) depicts the image of contact angle. The image is obtained for the sample after cleaning with piranha solution. The water profile on the slide is not like a drop, indicating that the free energy of surface is rather high. Hence, the surface exhibits high capability of chemical reaction. Figure 4.1(b) is the image for the surface immobilized with APTES. The contact angle is increased. The surface of slide after APTES treatment is covered with alkyl amino group, the surface becomes less hydrophilic than the surface without APTES. The detailed molecule immobilization on the surface is illustration in Scheme 4.1.



Scheme 4.1 The process flow for self-assembly.

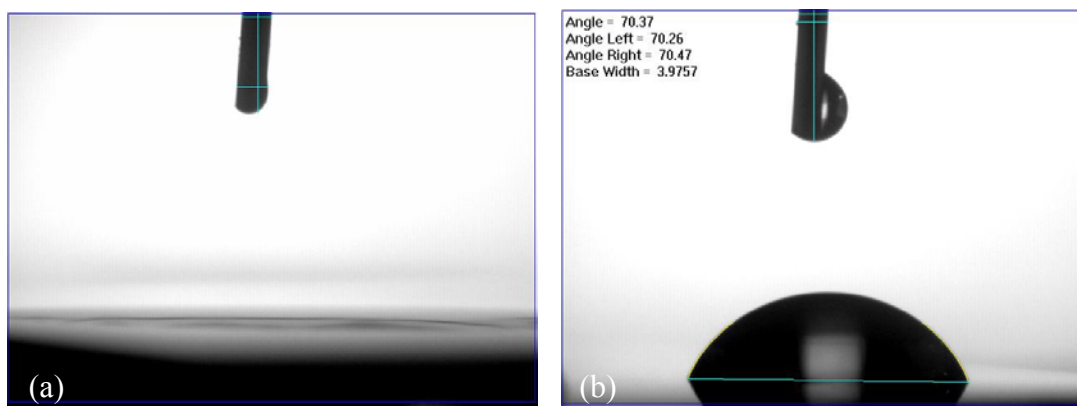


Figure 4.1. Images of contact angle: (a) after cleaning with piranha solution and (b) after APTES process.

Moreover, a polysilicon on oxide pattern was used to evaluate the surface reaction. We fabricated silicon dioxide/poly-silicon patterned slide by semiconductor process. The reason for this design is that the silicon dioxide substrate is a kind of oxygen-rich material; it will exhibit a lot of hydroxyl groups after treating with high oxidation of piranha solution (Piranha solution also called SPM solution, was made by H_2SO_4 and H_2O_2 (3:1); the solution possesses powerful oxidizing (organic destruction) capability. Silanol (Si-OH) groups on the surface were functionalized with APTES to form Si-O-Si bonding. After that, the reactive amino group was exhibited on the surface. We employed the rhodamine B isothiocyanate to confirm this above reaction. The free isothiocyanate functional group of rhodamine B isothiocyanate is active to amino group and we demonstrated the existence of amino group by detecting the fluorescence property of rhodamine group. As shown in figure 4.2(a), the chemical reaction between the amino groups of rhodamine B isothiocyanate and APTES assembled on the silicon dioxide substrate was illustrated. The amino group cleaves N=C bond of isothiocyanate, and forms two N-C bonding. Figure 4.2(b) shows the image of fluorescence microscopy, the bright fluorescent pattern confirms the reaction of rhodamine molecule onto the silicon dioxide. On the contrary, the poly-Si region does not emit red fluorescent pattern. As a result, we can confirm that APTES molecules are successfully assembled on the selected silicon oxide area of wafer.

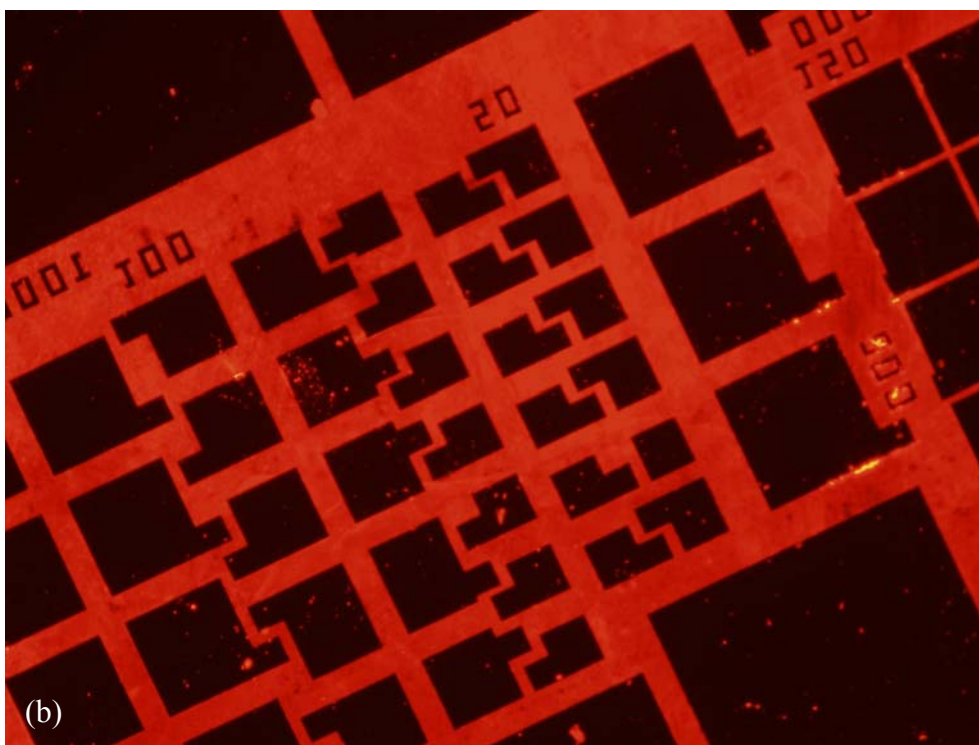
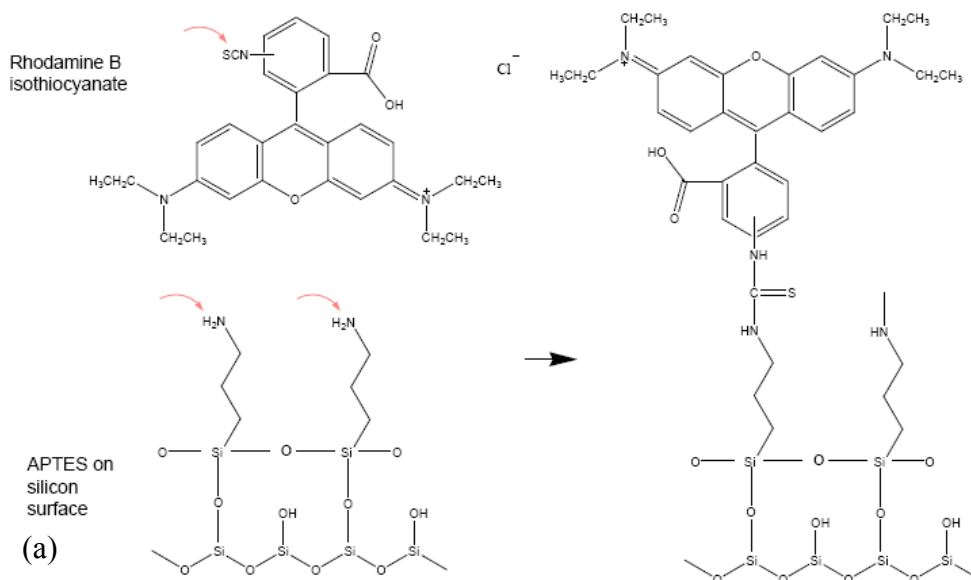


Figure 4.2. The patterned wafer of silicon oxide/poly silicon was immobilized with rhodamine B isothiocyanate. The materials of dark and bright areas were poly-silicon and silicon oxide, respectively. (a) APTES modified wafer reacts with rhodamine B isothiocyanate. (b) Fluorescence image of APTES/ rhodamine B isothiocyanate region.

We also attempt to optimize the binding of Biotin and streptavidin grafting steps.

Figure 4.3 denotes the images of APTES/NHS-biotin/Streptavidin(STA) system. We found that if the reaction time of APTES with NHS-biotin is only an hour, the reaction may not complete. However, the 6 hours reaction is suitable for the reaction. The result is in good accordance with many literatures [2].

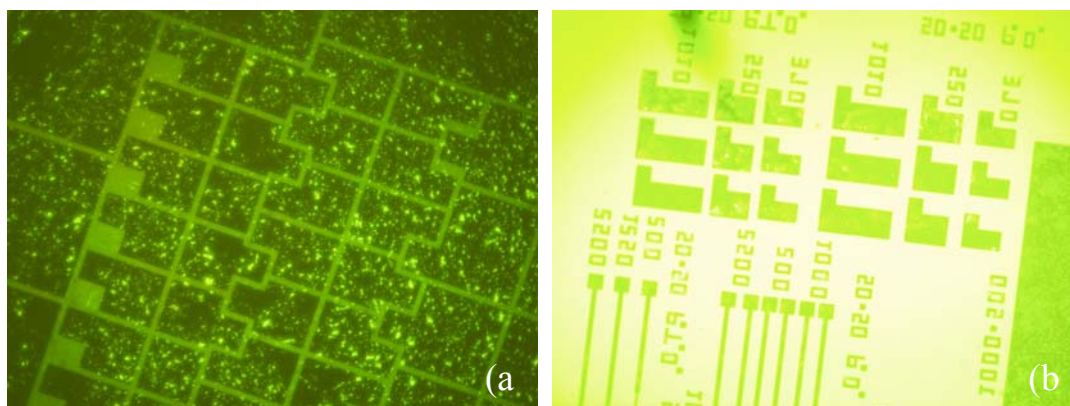
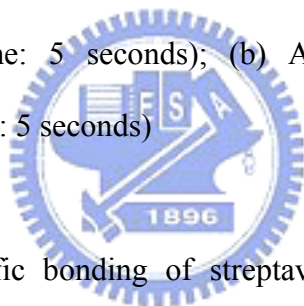


Figure 4.3. The images of fluorescence microscopy. (a) APTES/NHS-biotin (reaction time: 1 hour)/STA-Fitc (exposure time: 5 seconds); (b) APTES/NHS-biotin (reaction time: 6 hour)/STA-Fitc (exposure time : 5 seconds)



To reduce the non-specific bonding of streptavidin, we attempt to apply a further blocking step. Figure 4.4 shows the blocking experiment. Figure 4.4 (a) shows the black area (poly silicon) have a lot of spots, but figure 4.4 (b) shows that the patterns are obvious clear with applying the block reagent.

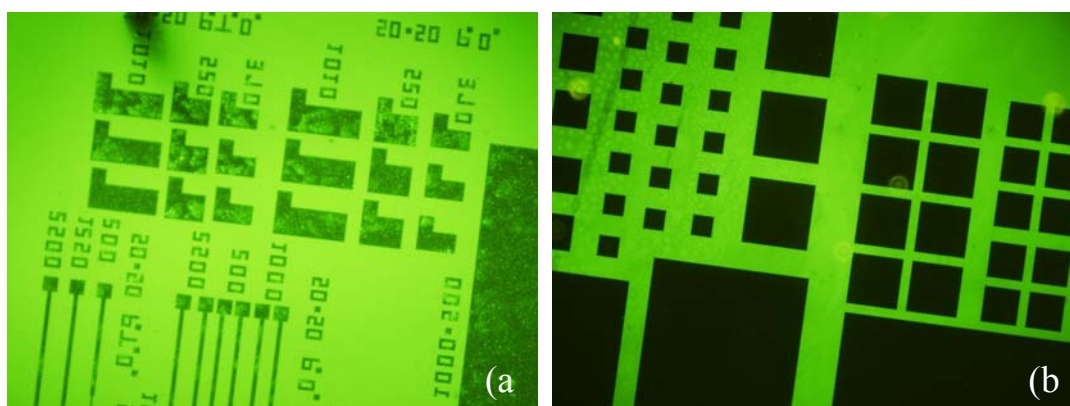
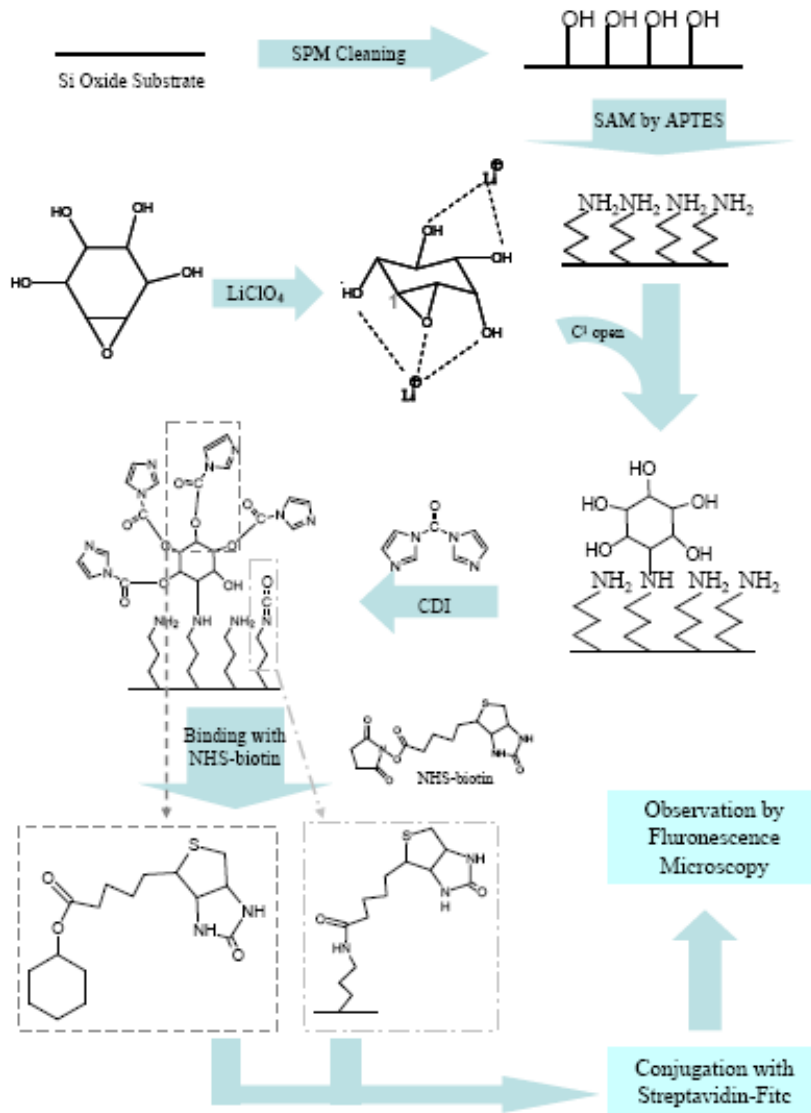


Figure 4.4. The images of fluorescence microscopy. (a) APTES/NHS-biotin (reaction time: 6 hour)/STA-Fitc (exposure time: 1 seconds) without blocking; (b) APTES/NHS-biotin

(reaction time: 6 hour)/STA-Fitc (exposure time: 1 seconds) with blocking.

4.2 Surface Modification by B Epoxide

In this thesis, we immobilized the epoxide onto the surface with APTES molecule, scheme 4.3 shows the detailed processing flow of immobilization.



Scheme 4.3 The processing flow of immobilization by B epoxide.

Figure 4.5 shows the images of fluorescence microscopy. There is no enhancement effect with modification by B epoxide, the reason could be that the B epoxide is not successfully binding with amino group of APTES. Although the literature shows the high yield (more than 90%) [3,4], it needs precise instruments and complicated reaction process. Furthermore, even

if the modification of B epoxide is fully covered on the surface, the reactivity of hydroxyl group on the B epoxide is not very high. The reaction is unfavorable for next conjugation. In summary, such immobilization can not contribute to a significant advance.

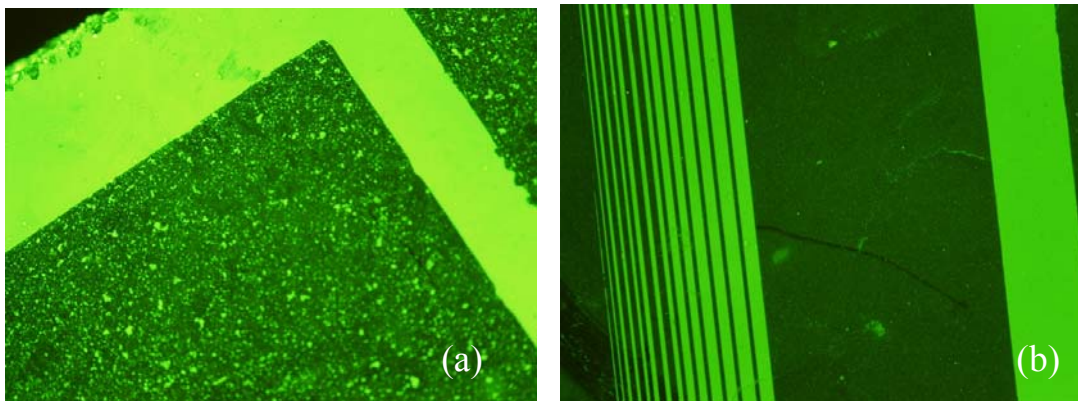
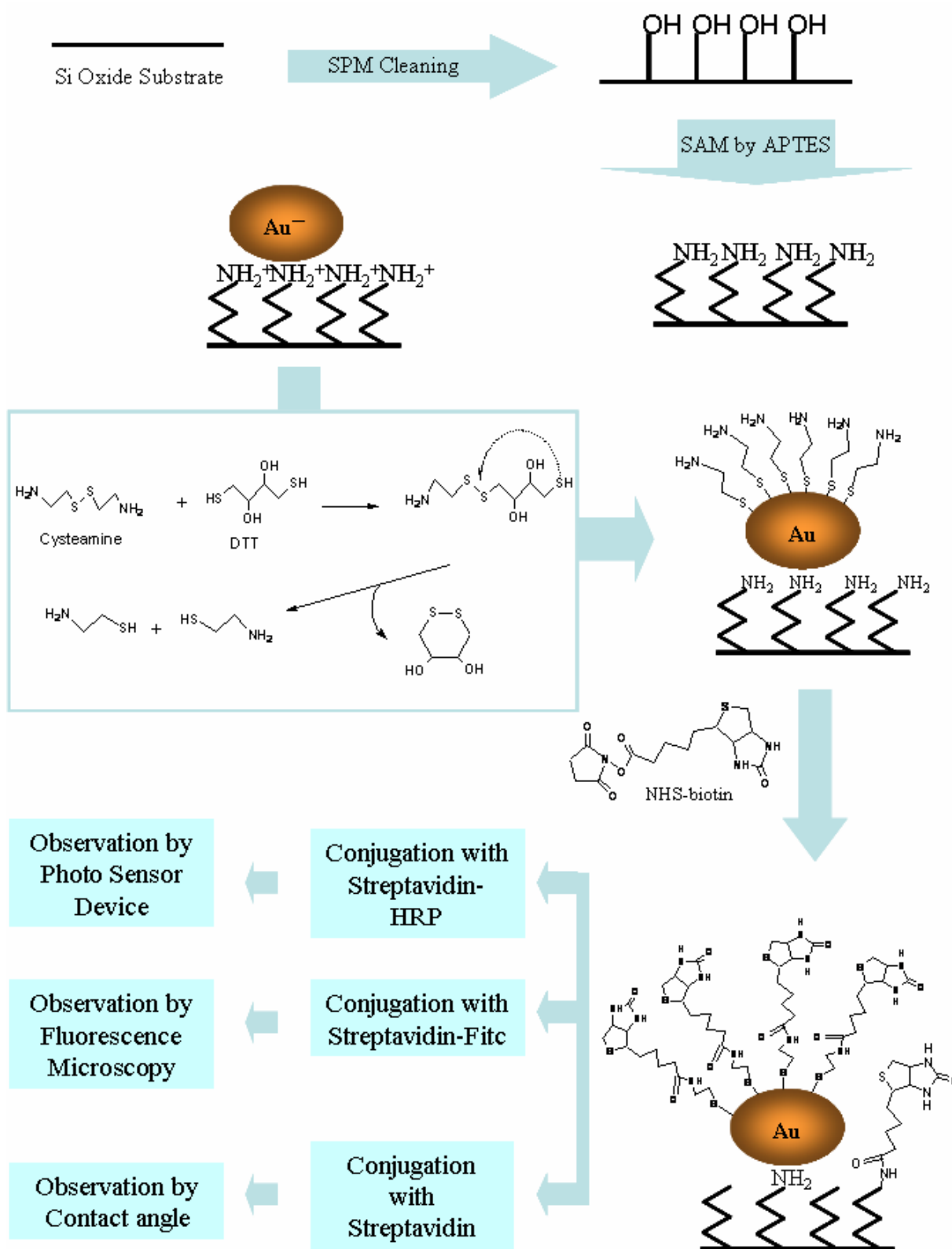


Figure 4.5. The images of fluorescence microscopy of (a) without modification, and (b) with modification by B epoxide.

4.3 Biotin-Streptavidin Conjugate with GNPs Assisted Modification

We have successfully prepared different sizes of gold nanoparticles by controlling the ratio of applying reagents. We use several instruments and software to confirm the size of gold nanoparticles. The scheme 4.4 shows the detailed processing flow of surface modification.



Scheme 4.4 The processing flow of modification by gold nanoparticles and cysteamine.

Firstly, we employed SEM (scanning electron microscopy) and IPP for confirming the size. There is a function of measurement in ancillary software of SEM, but requiring artificial

position fixing, and may cause serious personal inaccuracy. IPP (Image-Pro Plus) is the ultimate image analysis software package for fluorescence imaging, quality assurance, materials imaging. The software is widely accepted in various scientific researches such as medical and industrial applications. Count/size is one of the most useful function; it can measure the average or dispersion of diameter, area, and circumference, etc. This software greatly eliminates the inaccuracy, enabling us to measure the most accurate experimental data. As shown in figure 4.6(a), gold nanoparticles from SEM characterization was well dispersed by appropriate and careful sampling. No aggregation existed between gold nanoparticles. figure 4.6 (b) depicts the number-diameter diagram of gold nanoparticles, we can evaluate the distribution and mean size of gold nanoparticles.

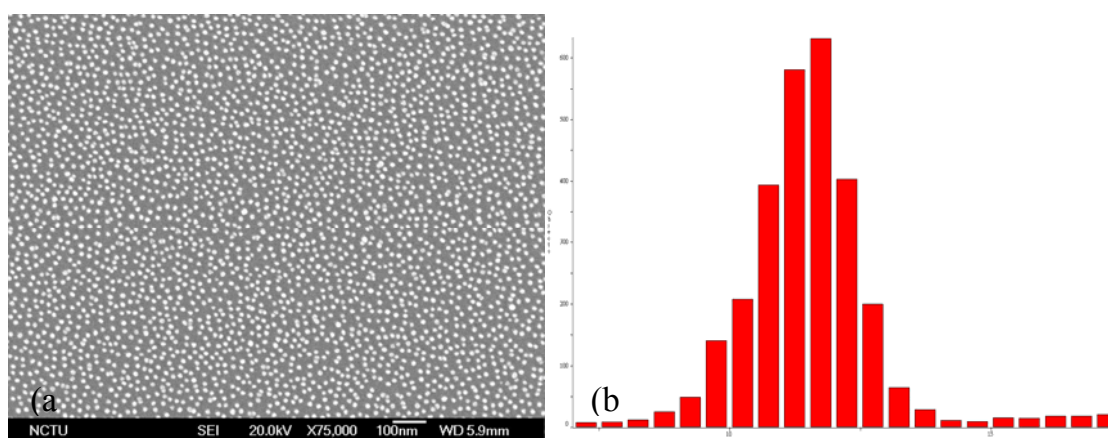


Figure 4.6. (a) The SEM image of gold nanoparticle; (b) number-diameter bar chart of gold nanoparticle.

Another method for diameter determination employed UV-visible spectrophotometer. UV-visible absorption spectra are useful for studying the properties of metal nanoparticles due to the sensitive peak positions and shapes in relation to the particle size and composition. When white light illustrated through or reflected by a color substance, a characteristic portion of the mixed wavelengths is absorbed. The remaining light will then assume the complementary color to the wavelength(s) absorbed. Thus, absorption of 420-430 nm light

renders a substance yellow, and absorption of 500-520 nm light makes it red. Green is unique in that it can be created by absorption close to 400 nm as well as absorption near 800 nm. Here, we use the above theory. Figure 4.7 shows the adsorption curve of different size of gold nanoparticles. The surface GNP density are $7.84 \times 10^{13} / \text{m}^2$ (20nm), $4.76 \times 10^{13} / \text{m}^2$ (45nm), $2.01 \times 10^{13} / \text{m}^2$ (60nm) and $1.14 \times 10^{13} / \text{m}^2$ (75nm), respectively.

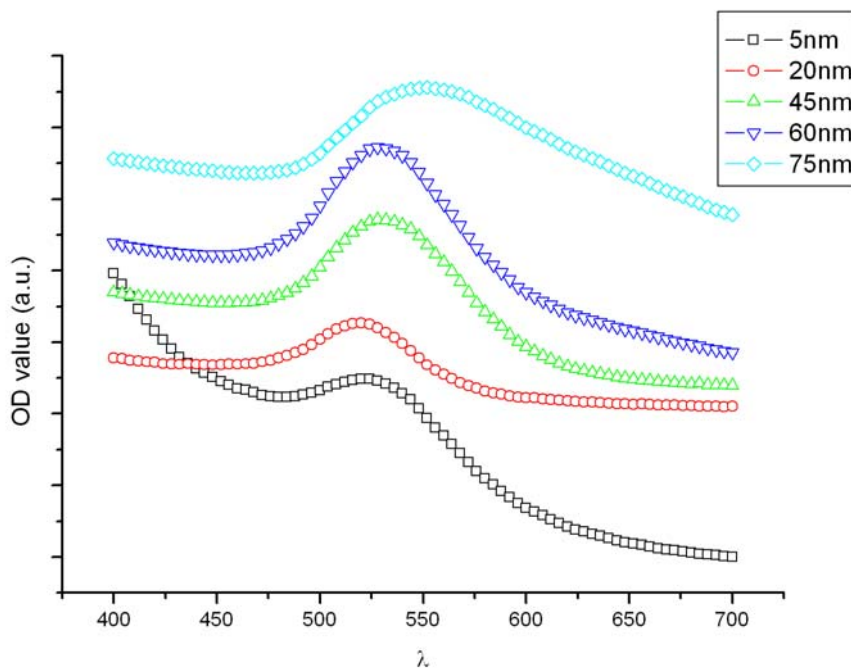


Figure 4.7. Absorbance spectra of different sizes of gold nanoparticles.

4.3.1 Characterization with Fluorescence Microscopy and IPP software

We studied the binding efficiency of streptavidin by gold nanoparticles assisted modification. In this thesis, we employed the fluorescence microscopy, UV-visible spectrophotometer and IV characterization to investigate the degree of enhancement.

Firstly, we verified several sizes of gold nanoparticle and chose the suitable size for the enhancement. Several sizes of gold nanoparticles were prepared: 5, 20, 45, 60, and 75 nm, in which the 20nm gold nanoparticle is commercial grand, the rest of the particles is prepared according to the literature [5,6].

Another important function for the IPP software is “histogram”, which can convert any information of image into a statistical chart. In this study, we have proposed standard procedure for the comparison of the illumination between several fluorescence images. The procedure were described as below:

Step 1 Open the image you want to deal with.

Step 2 Convert the colored image into grayscale mode image.

Step 3 Choose several area by the function “AOI” by avoiding the doubtful spots and areas.

Step 4 Definition these blocks by the function of “count/size”, determining which blocks will be calculated.

Step 5 Count the brightness of every pixel in blocks by the function of “histogram”.

Step 6 Export the data of step 6, than we can get the average brightness of a pixel.

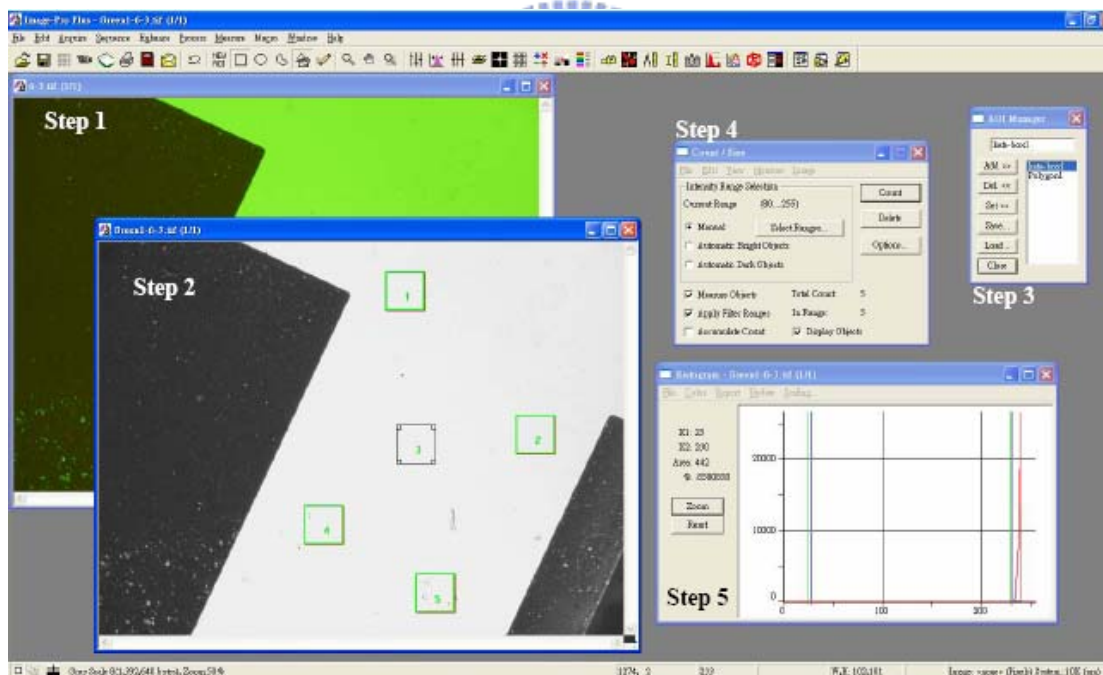


Figure 4.8. The diagram of brightness after quantification procedure.

As we know, the thio group will successfully immobilize onto the gold nanoparticles attached by APTES through the assistance of DDT. DDT will cleavage and restrain the formation of double sulfur bonding (S-S). Furthermore, there is no other active product after

reaction happened, indicating that there is no other disturbance in this reaction.

Figure 4.9 shows the bar chart for different sizes of gold nanoparticles that react with cysteamine but without DDT assistance. We found that there is no obvious difference for the groups without gold nanoparticles or with gold nanoparticles, except for 5 nm gold nanoparticle. The intensity was increased up when the DDT was participated with the reaction between cysteamine and gold nanoparticles (the result is at Figure 4.9). We found that the intensity of fluorescence was increased 58% between system without any modification and system with 20nm GNPs. The observation suggests gold nanoparticles and cysteamine can improve the binding efficiency. Besides, the area which did not cover with gold nanoparticles still possesses free amino groups that can react with NHS-biotin. Enhanced fluorescence of an organic fluorophore using nanoscale gold particles film was already investigated [7], Particulate gold films were deposited on glass substrates by vapor deposition. In this study, fluorescence was enhanced with increasing the Au thickness and reached saturation at 30 nm. The observation of literature supports our finding.

Another interesting phenomenon is also observed, the intensity of fluorescence at Figure 4.9 and Figure 4.10 both shows the system modification by 5nm gold nanoparticles having the lowest intensity of fluorescence. The Fluorescein has a maximum absorption at 494 nm and maximum emission at 521 nm. However, surface plasmon (SP) extinction band of hydrosol of 5 nm gold nanoparticles is at about 512 nm [8]. Hence, 5nm gold nanoparticle has higher extinction effect. Furthermore, 5nm gold nanoparticle has high aggregation effect. At the same reaction environment, 5nm gold nanoparticles have higher aggregation effect, and the reaction area was reduced when gold nanoparticles was aggregated.

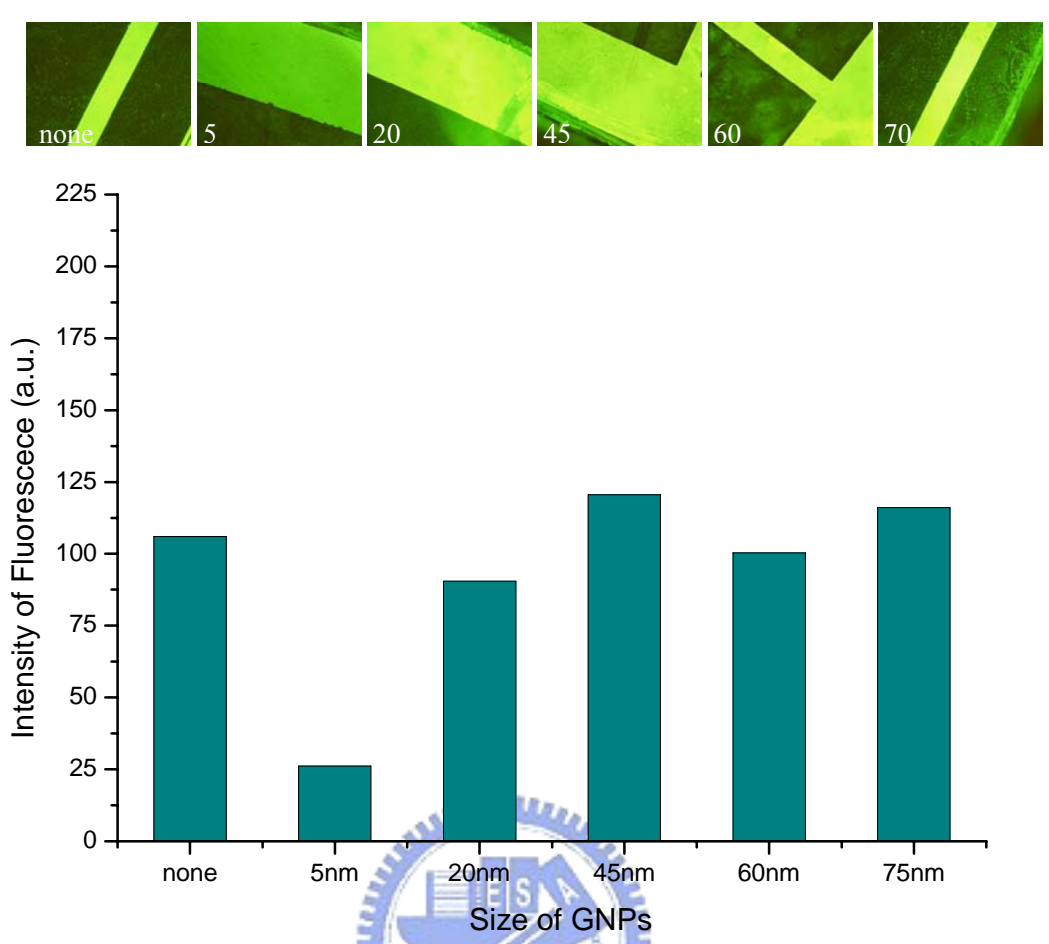


Figure 4.9. The bar chart of brightness after quantification.

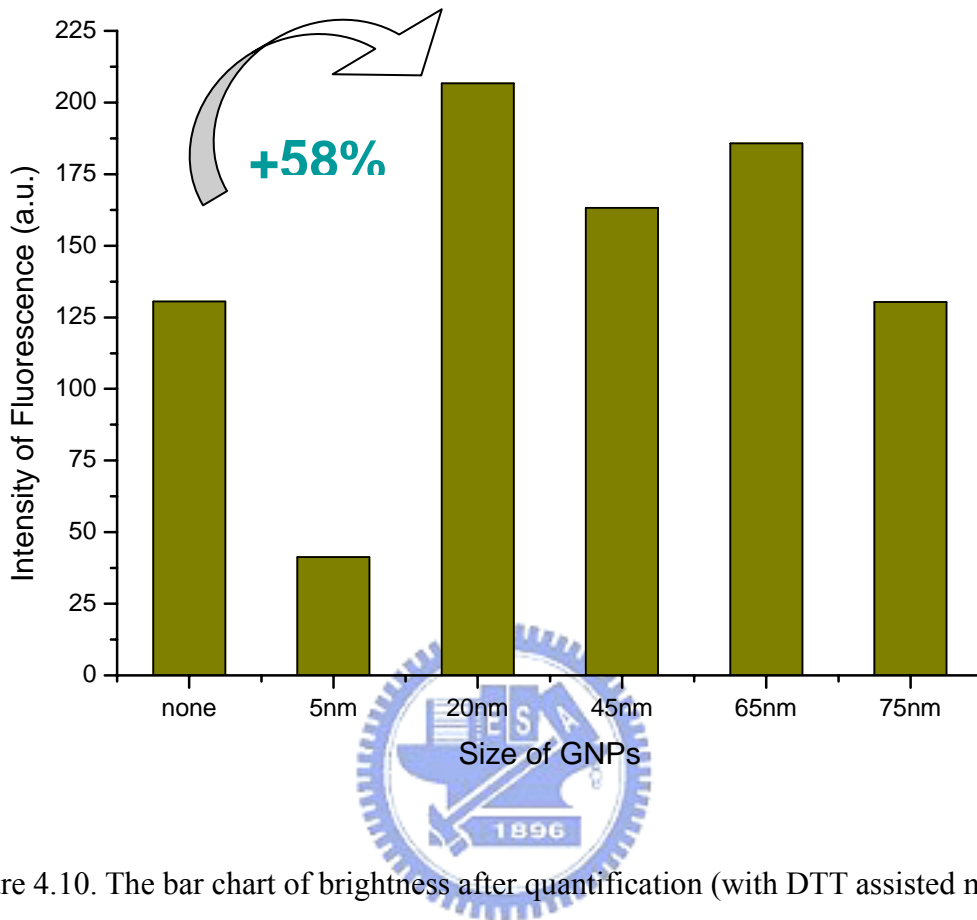
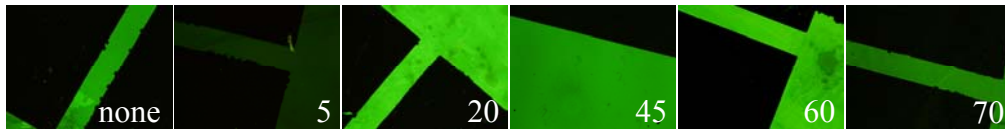


Figure 4.10. The bar chart of brightness after quantification (with DTT assisted modification).

We have also verified this system on bare Au film, and the results are shown in Figure 4.11. The intensity of fluorescence is 40 a.u. without any modification, but the value will elevate to 68 a.u. with GNPs assisted modification. The enhancement percentage is calculated to be $(68-40)/40= 70\%$.

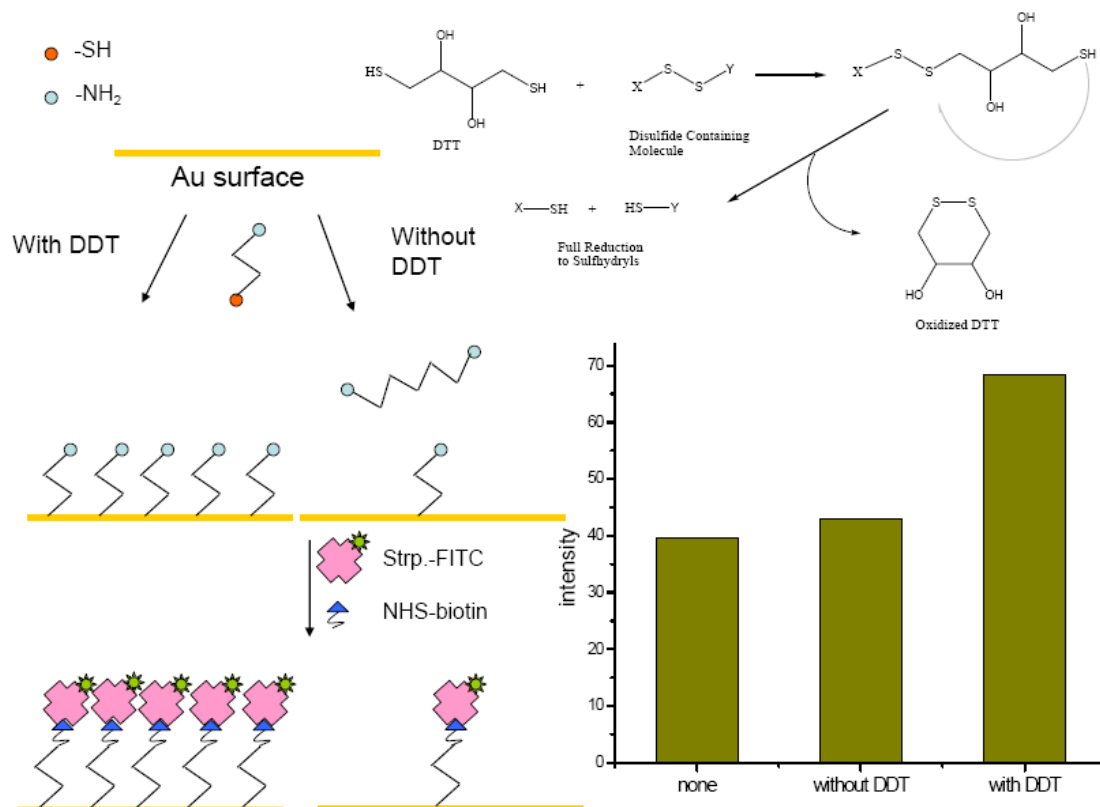


Figure 4.11. The bar chart of brightness after quantification. The graft of streptavidin-Fitc; without GNPs, with GNPs but without DTT and with GNPs plus DTT.

4.3.2 UV-Visible Spectrophotometer Evaluation

In this work, we study the effect of enhancement of GNPs and cysteamine by using the photonic property of luminol molecular. Luminol has notable absorption at wavelength of 350 nm [9]. When luminol reacts with H₂O₂ under the catalyst of HPR, the formed were produced and luminol concentration decreased gradually. The OD value of luminol is a rather suitable index for further application.

The preliminary test for luminol is shown in figure 4.12. The solid line is the absorption curve of luminol before reaction, and a significant absorption peak at 350 nm[10]. which is in accordance with literature. The dotted line is the absorption curve for luminol molecule that has reacted with HRP solution. The OD value at 350 nm was obviously decreased. This observation suggests the luminol molecules were have consumed.

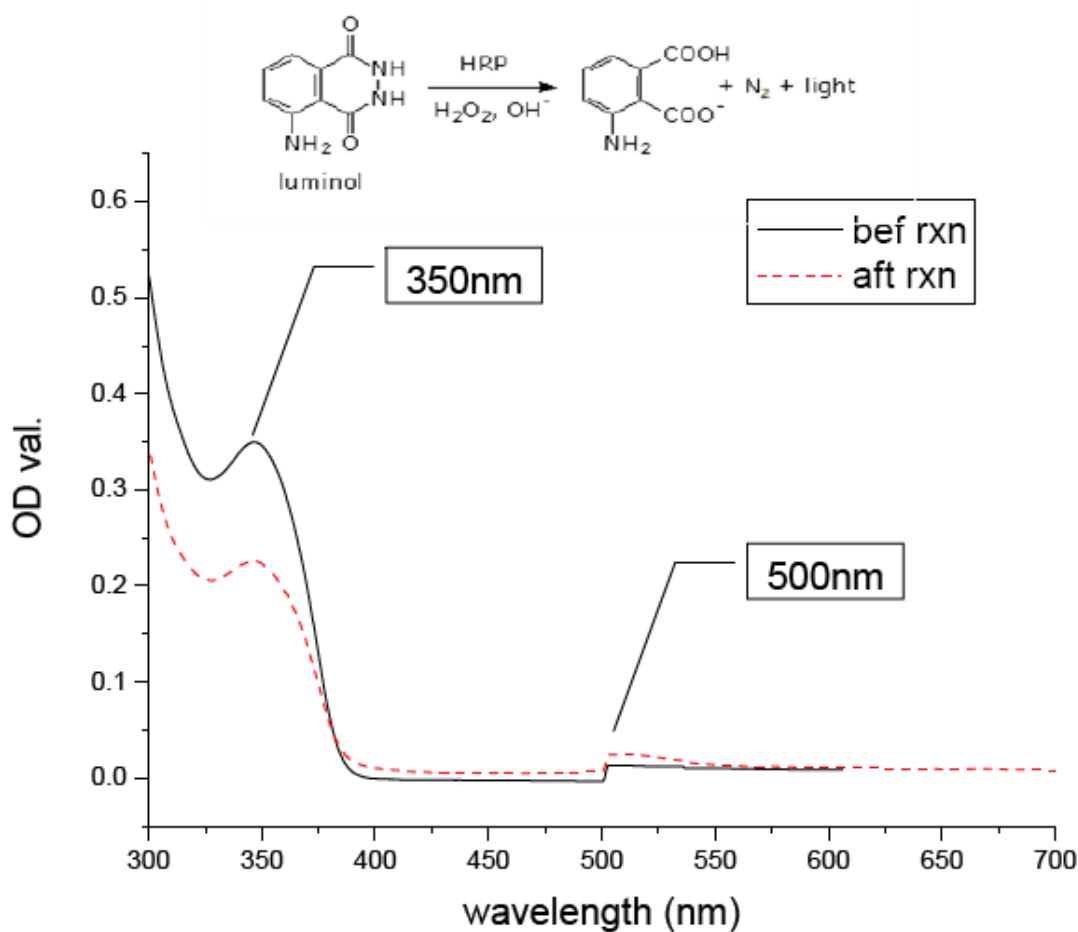


Figure 4.12. The OD value versus wavelength of absorption.

Furthermore, we prepared slides of silicon dioxide by semiconductor processing. We tried to stick the slides on two inside walls and ensure that the light does not pass through it.

The Figure 4.13 depicts the OD value with respect to wavelength of luminol at various times of 0, 30 minutes, 60 minutes, 90 minutes and 14 hours. Figure 4.13 (a) is the luminol reaction with HRP which has previously immobilized onto surface but without any further modification. The slides of which have surface modification have significantly higher rate of consumption. Figure 4.14 denotes the graph of OD value versus time. The solid line stands for the luminol reaction with immobilized HRP but without any modification. The dotted line stands for luminol reaction with immobilized HRP but with GNPs assisted modification. The literature has investigated the kinetics of luminol [11], and indicates the reaction of luminol is pseudo first order. The reaction rate is a constant according to their prediction, and the slope

of curve will be taken as reaction rate. After linear curve fitting, the slope of solid and dotted line are -0.0022 and -0.005 respectively, and the percentage of enhancement is $[(-0.005) - (-0.0022)] \div (-0.0022) \times 100\% = 127\%$.

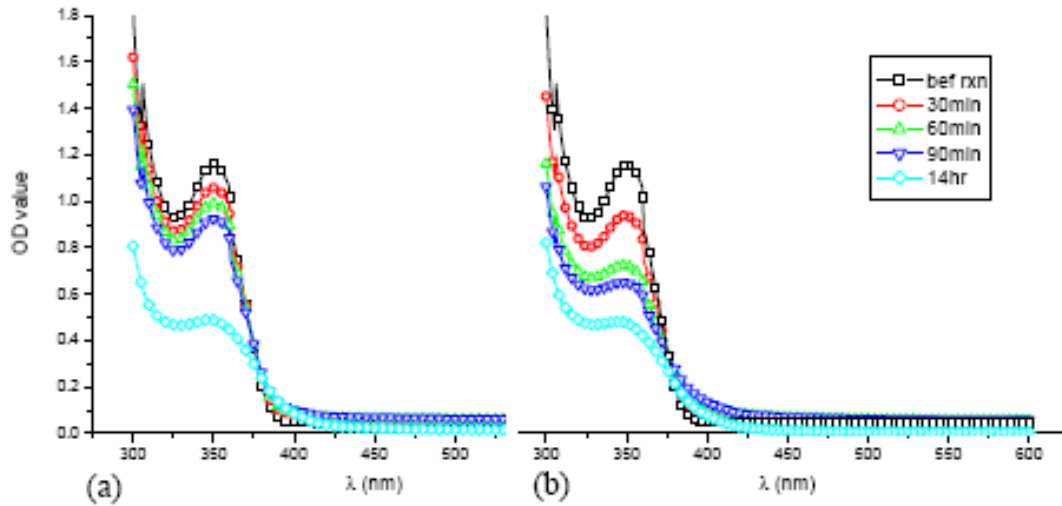


Figure 4.13. The OD value of luminal decay with reaction time. Conjugation of streptavidin-HRP without (a) and with (b) GNPs and cysteamine assistant.

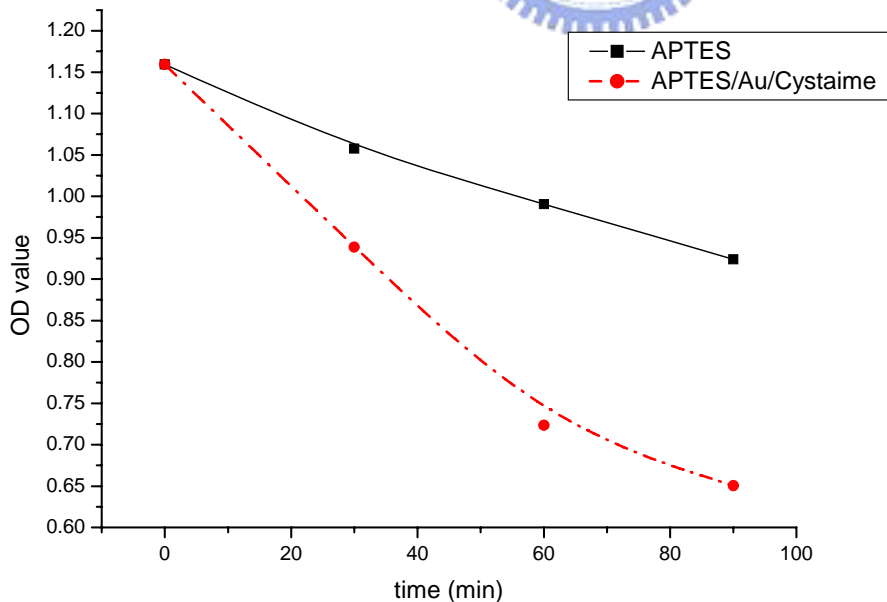


Figure 4.14. The OD value of luminal decay with reaction time. Conjugation of streptavidin-HRP without (a) and with (b) GNPs and cysteamine assistant.

4.3.3 Investigation by Photo Diode

A photodiode is a semiconductor diode that functions as a photodetector which nothing more than a bipolar transistor that is encased in a transparent case so that light can reach the base-collector junction. A photodiode is a p-n junction or p-i-n structure. When a photon of sufficient energy strikes the diode, it excites an electron thereby creating a mobile electron and a positively charged electron hole. If the absorption occurs in the junction's depletion region, or one diffusion length away from it, these carriers are swept from the junction by the built-in field of the depletion region, producing a photocurrent.

Photodiodes can be used under either zero bias (photovoltaic mode) or reverse bias (photoconductive mode). In zero bias, light falling on the diode causes a current across the device, leading to forward bias which in turn induces "dark current" in the opposite direction to the photocurrent. This is called the photovoltaic effect, and is the basis for solar cells — in fact; a solar cell is just a large number of big photodiodes.

Figure 4.15. shows the dark and photo current detected by photodiode. Prior to pouring luminol into the reaction tank, we detected dark current. The value of dark current is about 1.02×10^{-11} A. We detect the photo current once we pouring the luminol. The photo current was 2.63×10^{-10} ampere in the Si/APTES/NHS-biotin/Streptavidin-HRP system (Figure 4.15 (a)); the photo current was 2.63×10^{-9} ampere in the Si/APTES/GNPs/CysteamineNHS-biotin/Streptavidin-HRP system (Figure 4.15 (b)). The difference between the two system is one order of magnitude, this value is much bigger than the results in previous session. We suggest the reason of this phenomenon is that the photodiode is a kind of high sensitive electronic element which can clearly recognize the tiny difference between illumination. This result is much greater than the fluorescence microscopy.

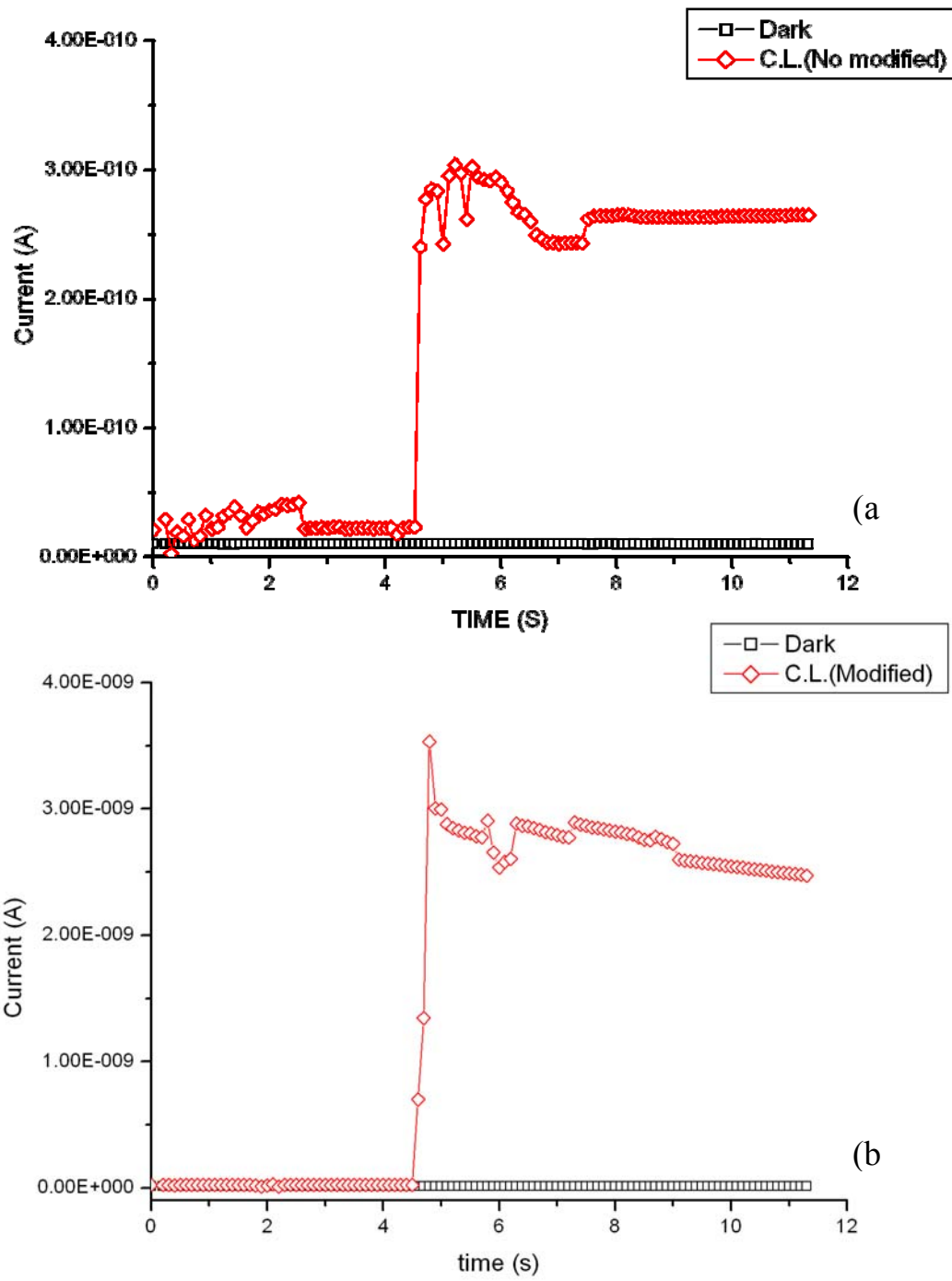


Figure 4.15. Real time measurement of chemiluminescence substrate. Without GNPs assistant immobilization; (b) with GNPs assistant immobilization.

4.4 Surface Energy for of Biomolecule Immobilization

The surface free energy of a solid can be used as a guide or indicator of its relative adhesive properties, it is difficult to measure the surface free energy of a solid directly. For practical reasons, procedures based on contact angle measurements are commonly employed. [12,13] The advancing contact angle is relatively less sensitive to surface roughness and heterogeneity than is the receding angle. Therefore, the advancing angle data are commonly used to calculate the components of surface and interfacial energy [14].

The surface free energy was evaluated by using van Oss and Good's three-liquid acid-base method [15]. According to this approach (refer to eq 1), the surface free energy of a solid, γ_S , can be calculated from a combination of three factors:

$$\gamma_S = \gamma_S^{LW} + \gamma_S^{AB} = \gamma_S^{LW} + 2\sqrt{\gamma_S^+ \gamma_S^-} \quad (1)$$

where γ^{LW} is the Lifshitz/van der Waals component, γ^{AB} is the acid-base component, γ^+ is the Lewis acid component, and γ^- is the Lewis base component. Values of γ^{LW} , γ^+ , and γ^- can be calculated from eq 2 after measuring the liquid-solid contact angles (θ) of these three characterizing liquids

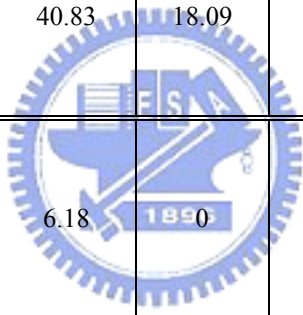
$$\begin{aligned} \gamma_{L1}(1 + \cos \theta_1) &= 2(\sqrt{\gamma_S^{LW} \gamma_{L1}^{LW}} + \sqrt{\gamma_S^+ \gamma_{L1}^-} + \sqrt{\gamma_S^- \gamma_{L1}^+}) \\ \gamma_{L2}(1 + \cos \theta_2) &= 2(\sqrt{\gamma_S^{LW} \gamma_{L2}^{LW}} + \sqrt{\gamma_S^+ \gamma_{L2}^-} + \sqrt{\gamma_S^- \gamma_{L2}^+}) \\ \gamma_{L3}(1 + \cos \theta_3) &= 2(\sqrt{\gamma_S^{LW} \gamma_{L3}^{LW}} + \sqrt{\gamma_S^+ \gamma_{L3}^-} + \sqrt{\gamma_S^- \gamma_{L3}^+}) \end{aligned} \quad (2)$$

In eq 2, γ_L is the surface tension of the liquid, and subscripts S and L refer to solid and liquid, respectively. Diiodomethane was selected as the apolar liquid, and water and ethylene glycol were selected as the polar liquid pair.

Table 4.1 shows the contact angles of water, ethylene glycol (EG), and diiodomethane (DIM) for each step of modified surface. It was obvious that the surface contact angle from polar solvents was significantly decreased after cleaning by SPM solution. This is attributed to hydrophilic hydroxide functional group. As to the surface assembled by APTES, the contact angle of polar solvents was descended and the contact angle of nonpolar solvent was

raised. The observation is explained by the hydrophobic amino functional group on the surface. Table 4.2 illustrates the calculated surface free energy. The surface energy is ranging from 47 mJ/cm² to 54 mJ/cm² for various surface. This observation suggests the various immobilization step can not significantly change the surface free energy. It is noted that the surface binding with biotin but without GNPs modification lower surface energy of 47 mJ/cm².

Table 4.1. The advancing contact angles for water, ethylene glycol (EG), and diiodomethane (DIM) on various modified surfaces.

	Without Modification			GNPs Assisting Modification		
	water	EG	DIM	water	EG	DIM
Bef. Cleaning	40.83	18.09	37.53	40.83	18.09	37.53
Cleaning by SPM	6.18		37.46	6.18	0	37.46
SAM by APTES	37.31	28.31	18.58	37.31	28.31	18.58
Conjugating with GNPs				15.27	22.89	25.53
Binding withth Cysteamine				54.47	27.03	25.4
Binding with Biotin	65.4	36.83	39.64	38.03	20.64	17.05

Binding with SA	26.52	18.88	24.7	39.04	23.96	35.21

Table 4.2. The corresponding surface free energies.

	Without Modification				GNPs Assisting Modification			
	γ_s^{LW}	γ_s^+	γ_s^-	γ_s	γ_s^{LW}	γ_s^+	γ_s^-	γ_s
Bef. Cleaning	40.8301	1.1156	32.4647	52.8913	41.0856	0.92741	36.98062	52.79857
Cleaning by SPM	40.8640	0.7225	57.9693	53.8184	40.86399	0.722544	57.96931	53.80777
SAM by APTES	48.1868	0.0703	38.1982	51.4652	48.18678	0.060362	39.40242	51.2712
Conjugating with GNP	/				45.9609	0.0615	58.4531	49.7519
Binding with Cysteamine					46.0081	0.6466	18.6725	52.9578
Binding with Biotin	39.7908	1.0855	11.1174	46.7388	48.5918	0.24523	35.3470	54.4802

Binding with SA	46.2585	0.2256	47.5294	52.8078	41.9309	0.6159	36.4168	51.4029
-----------------	---------	--------	---------	---------	---------	--------	---------	---------

4.5 Biosensing of Streptavidin by Real Time Optical Biosensor

In this section, the MSM-PD was demonstrated for detection the light emission from chemiluminescence. The chemiluminescence was catalyzed by HRP which conjugated on streptavidin molecules. The obtained signal represents the existence of streptavidin, and also confirms the existence of biotin. The detailed experimental process flow has described in chapter 3.2.

4.5.1 Real Time Sensing of Streptavidin by Detecting Chemiluminescence Applysis

In this section the MSM-PD was applied as biosensor for chemiluminescence detection. Figure 4.8 demonstrates the sensing system and the SEM image of the interdigitated fingers. In active area the metal lines are very close but independent; there will strong electric field between adjacent metal lines by applied electric potential on the metal pads. If the electrolysis is directly dropped onto the metallines, another current path thus increasing the dark current of the MSM-PD. The photo current to dark current ratio will be significantly drop ped and results in the difficult detection of photo current. Thus the silicon oxide layer was applied as blanked layer for completely avoiding the contact of electrolysis from liquid solution.

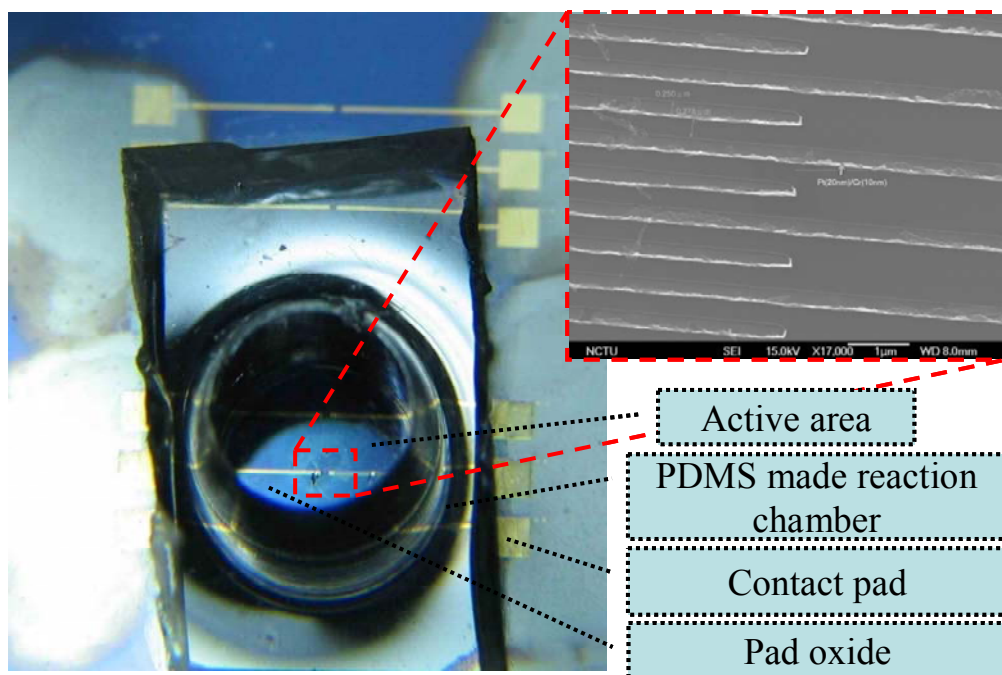


Figure 4.15. Chemiluminescence detection system.

The device is operated at 0.4V, and the light source is halogen lamp. The immobilization processes are all performed in reaction chamber (except for self assembly of APTES), thus will not change the contact resistance between probe and pad. The purpose of measuring photo response at each step is to make sure the device still works after each immobilization step. The dark current is 2nA and the photo current is 1.152uA after cleaning by piranha solution. The dark current slightly increase to 3.7nA, and the photo current is 193nA after immobilization by APTES. The photo current drop might because of light absorption effect by oxide chamber, and the measurement was under liquid solutions (PBS buffer). The solutions will also absorb some incident lights. The photo current is not concerned here, just to make sure the device is still work. The slight increment of dark current may attributed to leakage current results from oxide surface. The silicon oxide layer was deposited by PECVD (Plasma Enhanced Chemical Vapor Deposition system) process, and this may lead to some metal contamination and defects. Some ions in the liquid solutions near oxide surface might also exchange electrons and the electrons diffusion through defects in oxide layer then collected by metal electrodes. The leakage current causes slight increment of dark current. The results are shown at figure 4.9, figure 4.20, figure 4.11 and figure 4.12.

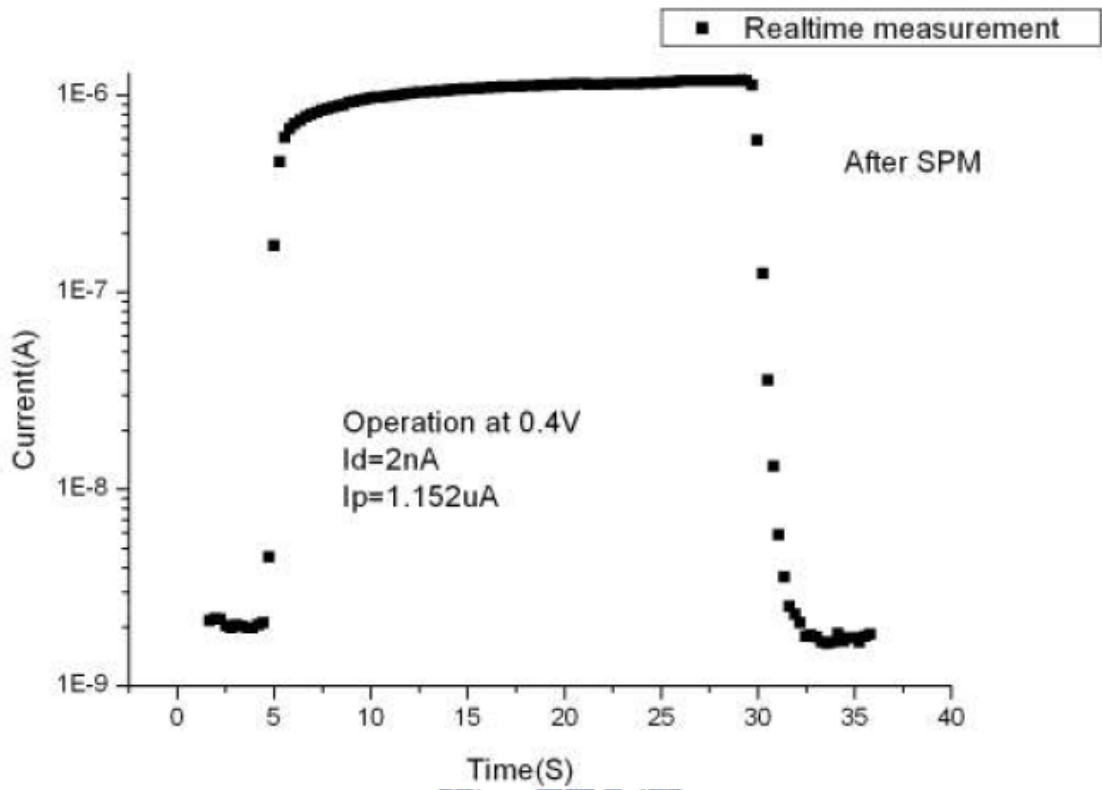


Figure 4.16. Current of MSM-PD after piranha solution.

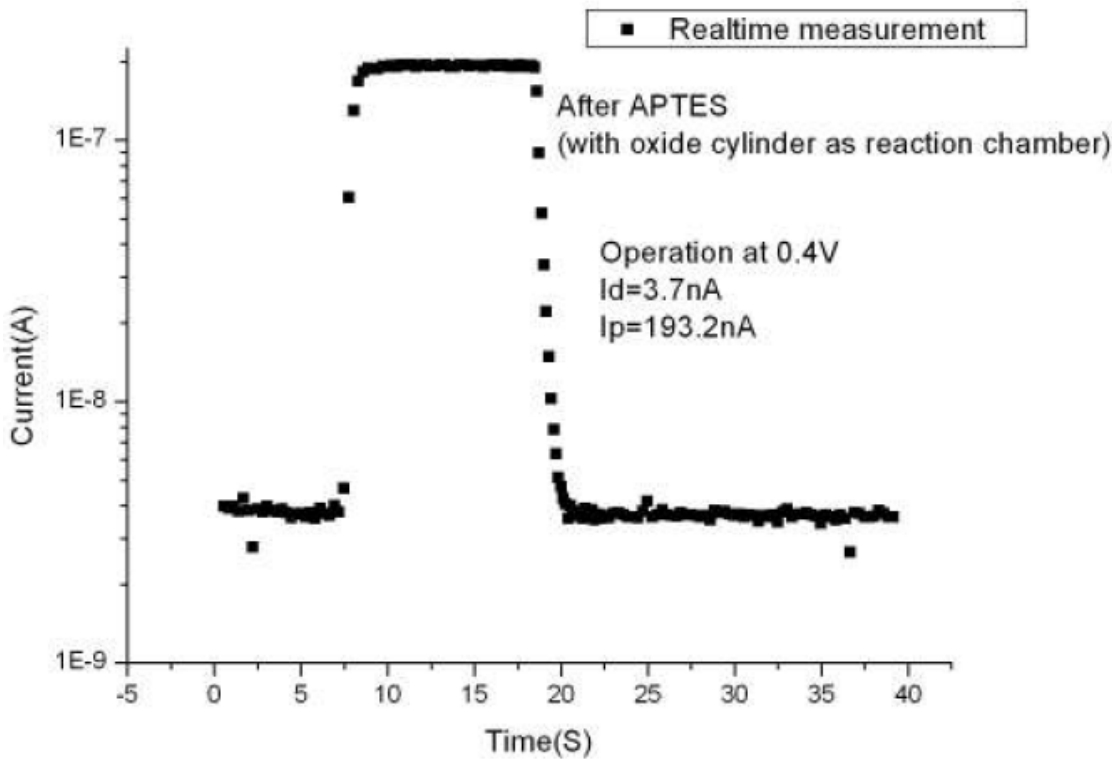


Figure 4.17. Current of MSM-PD after self assembling of APTES.

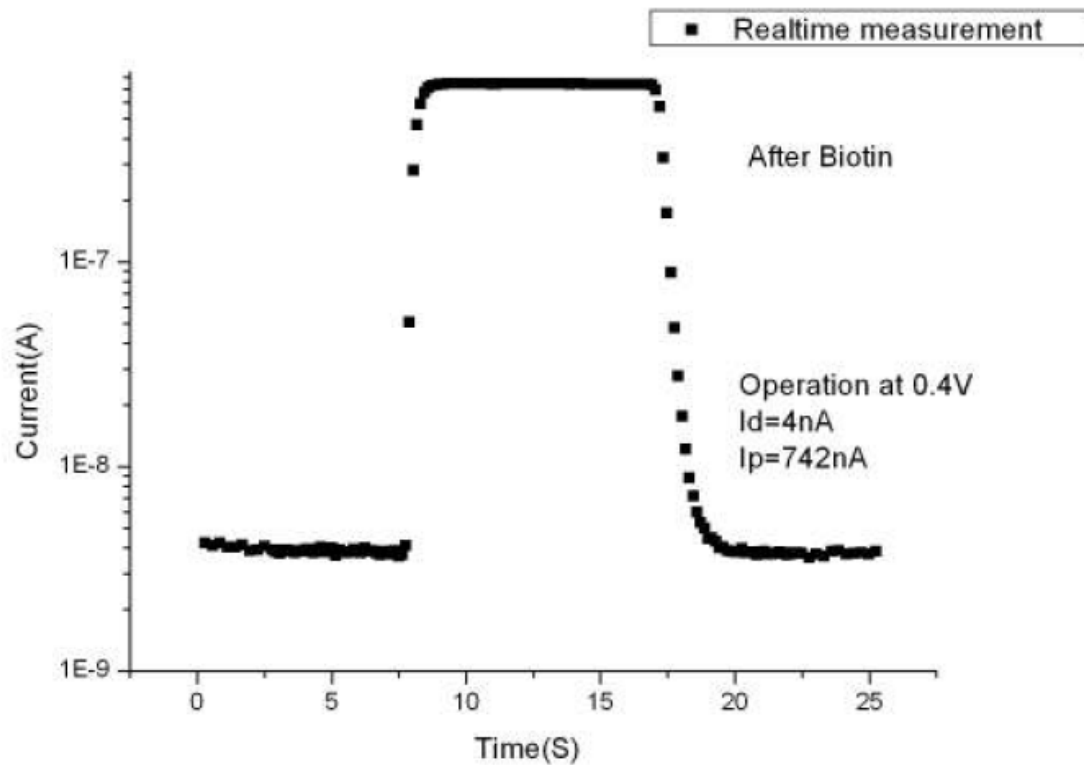


Figure 4.18. Current of MSM-PD after binding with NHS-bioth.

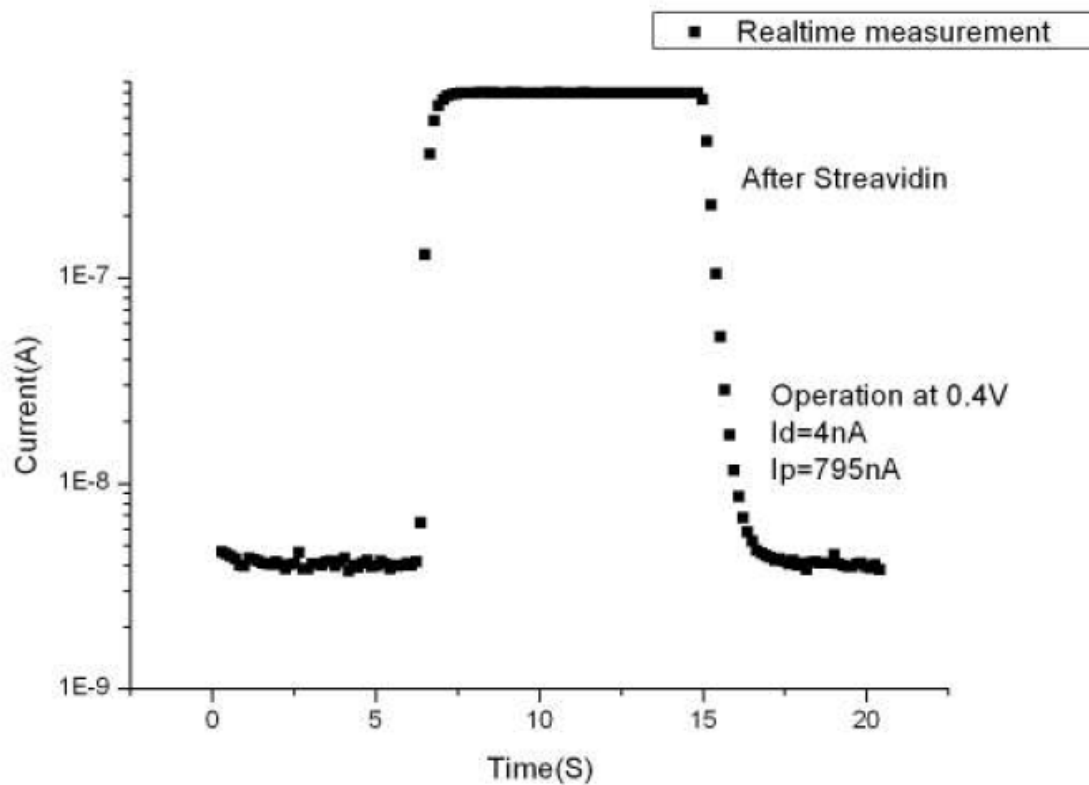


Figure 4.19. Current of MSM-PD after conjugating with streptavidin.

The following measurement was operated under liquid solutions (PBS buffer). The dark current was 4 nA after immobilization of biotin and conjugation between biotin and streptavidin. The emission of weak blue light was observation after adding substrate solutions (Chemiluminescent Peroxidase Substrate for Western Blotting; Sigma). The amount of streptavidin is 200ng and the volume solution is 200mL. The result is shown at figure 4.13, and there is a abruptly rise at 0 sec. The time of pouring of the substrate solution will simultaneously induce chemiluminescence in reaction chamber. The dark current and photo current are 0.45 nA and 1.98 nA respectively, and the value of I_p/I_d is $1.98 \div 0.45 = 4.4$. At the end of detection (140 sec.), the electronic current did not came back to initial value. The reason of this phenomenon is attributed to the continuous reaction between luminol and H_2O_2 was not stop. The amount of HRP catalyst was very tiny, but can maintain the reaction of system.

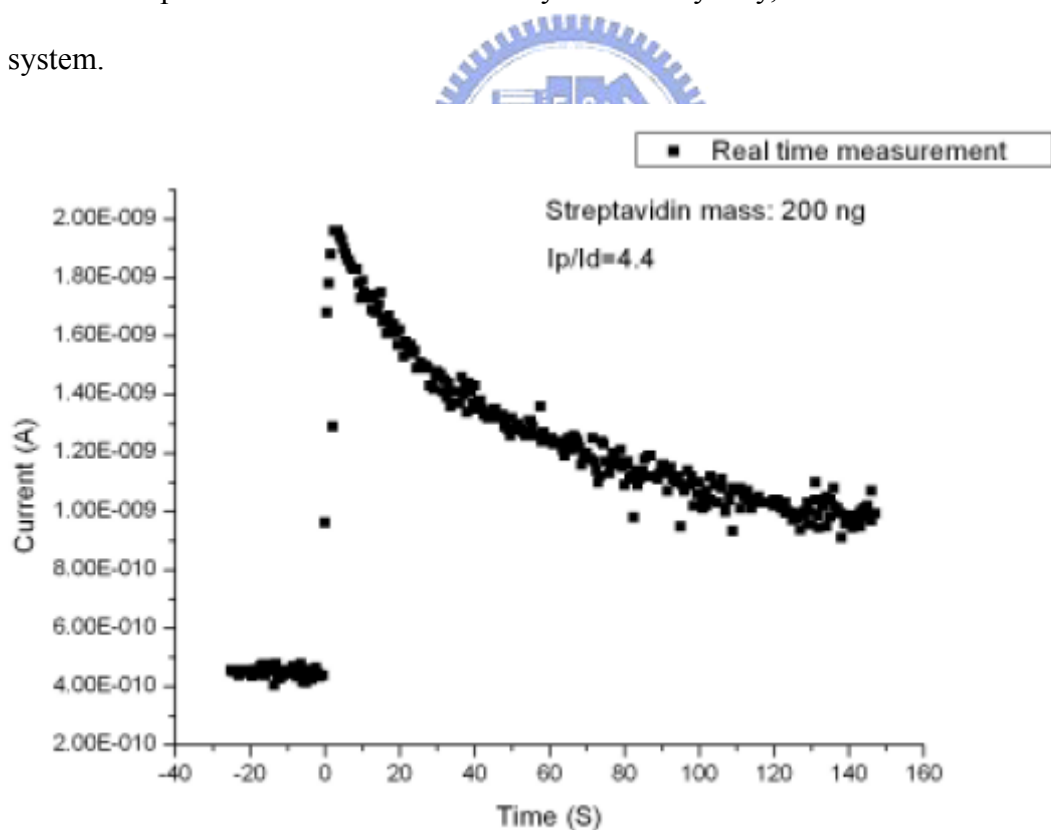


Figure 4.20. Real time measurement of adding chemiluminescence substrate of HRP (for detecting the streptavidin).

Chapter 5: Conclusions

The immobilization between the solid support and biomolecules is very important for the interdisciplinary studies of biotechnology and semiconductor fields. In this study, we firstly immobilize rhodamine by APTES modification onto silicon oxide substrates, and successfully investigated a fast and easy protocol to enhance the efficiency of immobilization. Furthermore, we successfully fabricated the metal-semiconductor-metal photo diode, and applied it on bio-sensing; it can be a very effective means to sense various important biomolecules. These devices also possess the advantages of very high sensitivity, label free and low cost.



Reference

Chapter 1: Introduction

1. T. Sakata & Y. Miyahara. "Detection of DNA recognition events using multi-well field effect devices." *Biosensors and Bioelectronics* 21, 827–832 (2005).
2. G. F. Zheng, F. Patolsky, Y. Cui, W. U. Wang, C. M. Lieber. "Multiplexed electrical detection of cancer markers with nanowire sensor arrays." *Nature biotechnology* 23, 1294-1301 (2005).
3. J. Justin Gooding, "Biosensor technology for detecting biological warfare agents:Recent progress and future trends". *Analytica Chimica Acta* 559, 137–151 (2006)
4. Lucilene Dornelles Mello, Lauro Tatsuo Kubota, *Food Chemistry* 77, 237–256 (2002)
5. Daniel R. The'venot , Klara Toth, Richard A. Durst and George S. Wilson, "Electrochemical biosensors: recommended definitions and Classification", *Biosensors & Bioelectronics* 16, 121–131 (2001)
6. chemical sensors and biosensors. Brian R. Eggins
7. Bin Xie, Michael Mecklenburg and Ben Danielsso, "Development of an Integrated Thermal Biosensor for the Simultaneous Determination of Multiple Analytes", *Analyst* 120, 155-160 (1995)
8. "Biosensors: Fundamentals and Applications", A. P. F. Turner and G. S. Wilson by permission of Oxford University Press, (1987)
9. L. Raleigh, *Proc. R. Soc. Lond. A, Math Phys. Sci.* 17, 4-11 (1885).
10. Curie J and Curie P 1880 D'veloppement, par pression, de l'electricit'e polaire dans les cristaux h'emi`edres `a faces inclin'ees *C. R. Acad. Sci., Paris* 91 294-5

11. C.K. O'Sullivan and G.G. Guilbault, "Commercial quartz crystal microbalances – theory and applications", *Biosensors & Bioelectronics*, 14, 663-670, (1999)
12. Aumuller G, Seitz J. 1988. Immunocytochemical localization of actin and tubulin in rat testis and spermatozoa. *Histochemistry* 89, 261-267.
13. Aumuller G, Seitz J. 1988. Immunocytochemical localization of actin and tubulin in rat testis and spermatozoa. *Histochemistry* 89: 261-267.
14. Homola J.; Yee S.S.; Gauglitz G. "Surface plasmon resonance sensors", *Sensors and Actuators B: Chemical*, Volume 54, Number 1, 25 January 1999 , pp. 3-15(13)
15. Bataillard P, Steffgen E, Haemmerli S, Manz A, Widmer HM. "An integrated silicon thermophile as biosensor for the thermal monitoring of glucose, urea and penicillin.", *Biosens Bioelectron.* 1993;8(2):89-98.
16. BLUM L. J., GAUTIER S. M, COULET P. R, "Luminescence fiber-optic biosensor", *Analytical letters*, 1988, vol. 21, no5, pp. 717-726
17. Bostrom Caselunghe M and Lindeberg J., "Biosensor-based determination of folic acid in fortified food", *Food Chemistry*, 70, 4, 523-532 (2000)
18. Monzir S. Abdel-Latif and George G. Guilbault, *Fiber-optic Sensor for the Determination of Glucose Using Micellar Enhanced Chemiluminescence of the Peroxyoxalate Reaction*", *Anal. Chem.* 1008, 60, 2677-2674
19. Eggins, B. R., *Biosensors: An Introduction*, John Wiley & Sons Limited, (1966).
20. Hall, E. A. H., *Biosensors*, John Wiley & Sons Limited, (1990).

Chapter 2: Literatures Review

1. Y. Ji, V. Toader, B. M. Bennett. "Regulation of microsomal and cytosolic glutathione S-transferase activities by S-nitrosylation." *Biochem. Pharmacol.* 63, 1397-1404 (2002).
2. <http://en.wikipedia.org/wiki/Luminol>

3. <http://en.wikipedia.org/wiki/Luminol#Chemiluminescence>
4. Klaus Buchholz, Volker Kasche and Uwe T. Bornscheuer. "Biocatalysts and Enzyme Technology", Wiley-Vch
5. Ana M. Garcia Campana and Willy R. G. Byeyens, "Chemiluminescence in Analytical Chemistry".
6. S. J. Tans, A. R. M. Verschueren, C. Dekker. "Room-temperature transistor based on a single carbon nanotubes." *Nature* 393, 49-52 (1998).
7. G. Maruccio, A. Biasco, P. Visconti, A. Bramanti, P. P. Pompa, F. Calabi, R. Cingolani, R. Rinaldi, S. Corni, R. Di Felice, E. Molinari, M. P. Verbeet, G. W. Canters. "Towards protein field-effect transistors: report and model of a prototype." *Adv. Mater.* 17, 816-822 (2005).
8. J. Appenzeller, J. Knoch, V. Derycke, R. Martel, S. Wind, P. Avouris. "Field-modulated carrier transport in carbon nanotube transistors." *Phys. Rev. Lett.* 89, 126801 (2002).
9. R. F. Wolffenbutte. "Low-temperature intermediate Au-Si wafer bonding; eutectic or silicide bond." *Sensors and Actuators A* 62, 680-686 (1997).
10. M. Hansen, K. Anderko. *Constitution of Binary Alloy*, 2nd ed. (McGraw-Hill, New York, 1958).
11. J. F. Chang, T. F. Young, Y. L. Yang, H. Y. Ueng, T. C. Chang. "Silicide formation of Au thin films on (100) Si during annealing." *Materials Chemistry and Physics* 83, 199-203 (2004).
12. S. R. Das, K. Sheergar, D. X. Xu, A. Naem. "Thickness dependence of the properties and thermal stability of PtSi films." *Thin Solid Films* 253, 467 (1994).
13. Q. Z. Hong, S. Q. Hong, F. M. D'Heurle, J. M. E. Harper. "Thermal stability of silicide on polycrystalline Si." *Thin Solid films* 253, 479 (1994).
14. T. Sano, S. Vajda, C. R. Cantor. "Genetic engineering of streptavidin, a versatile affinity tag." *Journal of Chromatography B* 715, 85-91 (1998).
15. W. A. Hendrickson, A. Pahler, J. L. Smith, Y. Satow, E. A. Merritt, R. P. Phizackerley. "Crystal structure of core streptavidin determined from multiwavelength anomalous diffraction of synchrotron radiation." *Proc. Natl.*

- Acad. Sci. USA 86, 2190-2194 (1989).
16. D. Pacheco-Alvarez, R. S. Solórzano-Vargas, A. León Del Río. "Biotin in metabolism and its relationship to human disease." *Archives of Medical Research* 33, 439-447 (2002).
 17. Janeway CA, Jr. et al. *Immunobiology*, 6th ed. (Garland Science, 2005).
 18. K. F. Karpinski. "Optimality assessment in the enzyme-linked immunosorbent assay (ELISA)." *Biometrics* 46, 381-390 (1990).
 19. N. Ida, T. Hartmann, J. Pante, J. Schröder, R. Zerfass, H. Förstl, R. Sandbrink, C. L. Masters, K. Beyreuther. "Analysis of heterogeneous β A4 peptides in human cerebrospinal fluid and blood by a newly developed sensitive western blot assay." *The Journal of Biological Chemistry* 271, 22908-22914 (1996).
 20. F. H. Ko, Z. H. Yeh, C. C. Chen, T. F. Liu. "Self-aligned platinum-silicide nanowires for biomolecule sensing." *J. Vac. Sci. Technol. B* 23, 3000-3005 (2005).
 21. *Bioconjugate Techniques*, Greg T. Hermanson, 77-79 (1996)
 22. V. H. Lillelund, H. H. Jensen, X. F. Liang, M. Bols, *Chem. Rev.*, 102, 515 -553 (2002).
 23. A. Berecibar, C. Grandjean, A. Siriwardena, *Chem. Rev.*, 99, 779-844 (1999).
 24. Pedro Serrano, Amadeu Llebaria, Jordi V&zquez, Joan de Pablo, Josep M. Anglada, and Antonio Delgado. "On the Regio- and Stereoselective Synthesis of Aminocyclitols from Cyclitol Epoxides: The Effect of Li as a Chelating Agent". *Chem. Eur. J.* 11, 4465-4472 (2005)
 25. M. Bartok, K. L. Lang, in *Small Ring Heterocycles* (Ed.: A. Hassner), Wiley, New York, 1985.
 26. F. Calvani, P. Crotti, C. Gardelli, M. Pineschi," Regiochemical control of the ring opening of 1,2-epoxides by means of chelating processes. 8. Synthesis and ring

- opening reactions of cis- and trans- oxides derived from 3-benzyloxycyclohexene and 2-benzyloxy-5,6-dihydro-2H-pyran”, Tetrahedron 50, 12999-13022 (1994).
27. Meritxell Egido-Gab, Pedro Serrano, Josefina Cas, Amadeu Llebariaa and Antonio Delgado. “New aminocyclitols as modulators of glucosylceramide metabolism”, Org. Biomol. Chem., 3, 1195-1201 (2005)
28. W. Schottky, “Halbleiterttheorie der sperrschicht,” Naturwissenschaften, 26, 843 (1938).
29. S. M. Sze, Physics of Semiconductor Devices, 2nd Ed., John Wiley & Sons, New York, (1981)
30. E. H. Rhoderick, “Metal-semiconductor contacts,” IEE Proc., 129, 1 (1982).
31. E. H. Rhoderick and R. H. Williams, Metal-Semiconductor Contacts, 2nd Ed., Clarendon Press, Oxford, (1988).
32. W. Schottky and E. Spenke, “Quantitative treatment of the space charge and boundary-layer theory of the crystal rectifier.”, Wiss. Veroff. Siemens-Werken., 18, 225 (1939).
33. E. Spenke, Electronic Semiconductors, McGraw-Hill, New York, (1958).
34. H. A. Bethe, “Theory of the boundary of crystal rectifiers.”, MIT Radiation Lab. Rep. 43-12 (1942).
35. C. R. Crowell and S. M. Sze, “Current transport in metal-semiconductor barriers.”, Solid State Electron., 9, 1035 (1966).
36. A. M. Cowley and S. M. Sze, “Surface states and barrier height of metalsemiconductor systems.”, J. Appl. Phys., 36, 3212 (1965).

Chapter 4: Results and Discussion

1. Wilchek, M., and Bayer, E. A. Anal. Biochem. 171, 1-32 (1988)

2. Katrien De Vos, Irene Bartolozzi, Etienne Schacht, Peter Bienstman and Roel Baets, "Solicon-on-Insulator microring resonator for sensitive and label-free biosensing". OPTICS EXPRESS 15, 12, 7613-7615 (2007)
3. F. Calvani, P. Crotti, C. Gardelli, M. Pineschi, "Regiochemical control of the ring opening of 1,2-epoxides by means of chelating processes. 8. Synthesis and ring opening reactions of cis- and trans- oxides derived from 3-benzyloxycyclohexene and 2-benzyloxy-5,6-dihydro-2H-pyran", Tetrahedron, 50, 12999-13022 (1994).
4. Meritxell Egido-Gab, Pedro Serrano, Josefina Cas, Amadeu Llebariaa and Antonio Delgado. "New aminocyclitols as modulators of glucosylceramide metabolism", Org. Biomol. Chem., 3, 1195-1201 (2005)
5. Sihai Chen and Keisaku Kimura, "Synthesis and Characterization of Carboxylate-Modified Gold Nanoparticle Powders Dispersible in Water", Langmuir, 15 (4), 1075 -1082 (1999).
6. S. J. Park, S. Kim, S. Lee, "Synthesis and Magnetic structure of uniform Iron nanorods and nanospheres.", Journal of the American Chemical Society 122, 8581-8582 (2000)
7. Wilchek, M., and Bayer, E. A. Anal. Biochem. 171, 1-32 (1988)
8. Jian Zhang and Joseph R. Lakowicz, "Metal-enhanced fluorescence of an organic fluorophore using gold particles", OPTICS EXPRESS 15(5), 2598~2606 (2007)
9. Martin M. F. Choi, "Progress in Enzyme-Based Biosensors Using Optical", Microchimica Acta 18 107-132.
10. P. Zhang and T. K. Shan, Appl. Phys. Lett., 81, 736 (2002); Y. J. Huang, D. Li, and J. H. Li, Chem. Phys. Lett., 389, 14 (2004).
11. <http://www.chm.bris.ac.uk/webprojects2002/fleming/experimental.htm>
12. Zisman, W. A. Ind. Eng. Chem. 1963, 55, 18
13. Fowkes, F. M. J. Phys. Chem. 1962, 66, 382.

14. Good, R. J.; van Oss, C. J. Modern Approaches to Wettability: Theory and Applications; Schrader, M. E., Loeb, G., Eds.; Plenum Press: New York, 1-27 (1992).
15. Van OCJ, Chaudhury MK, Good R J. "Interfacial Lifshitz-van der Waals and polar interaction in macroscopic systems." Chem Rev 88, 927-941 (1988)

